Forecasting the Confirmed COVID-19 Cases Using the Modal Regression

XIN JING
School of Economics, Yonsei University, Seodaemun-gu, Seoul 03722, Korea
Email: superheunheun@gmail.com

JIN SEO CHO
School of Economics, Yonsei University, Seodaemun-gu, Seoul 03722, Korea
Email: jinseocho@yonsei.ac.kr

This version: May 23, 2023

Abstract

The current paper utilizes modal regression to forecast the cumulative confirmed COVID-19 cases for Canada, Japan, Korea, and the U.S. The objective is to improve the accuracy of the forecasts compared to standard mean and median regressions. To evaluate the performance of the forecasts, we conduct simulations and introduce a metric called the coverage quantile function (CQF), which is optimized by the modal regression. By applying the modal regression to popular time-series models for COVID-19 data, we provide empirical evidence that the forecasts generated by the modal regression outperform those produced by the mean and median regressions in terms of the CQF. This finding addresses the limitations of the mean and median regression forecasts.

Key Words: Forecasting COVID-19 cases; Modal regression; Conditional mode; MEM algorithm; Density estimation.

JEL Classifications: C22, C53, I18.

Acknowledgements: The authors are grateful to Jihye Jung, Jaeseung Lee, and Moo Hyun Yang for constructive comments.

1 Introduction

Since the first confirmed identification of coronavirus disease (COVID-19) in Wuhan, China, in December 2019, it has emerged as a global concern. The World Health Organization (WHO) declared it a global pandemic on March 11, 2020. By April 2022, there had been over 500 million confirmed cases and 6 million deaths worldwide. Given the seriousness of COVID-19, numerous countries swiftly implemented various measures, including short-term actions like lockdowns, as well as long-term strategies such as social distancing and vaccine development.

The economic impact of COVID-19 has been severe, leading governments worldwide to respond with significant budget expenditures. As depicted in Table 1, governments have employed various measures to combat COVID-19, resulting in substantial budget allocations. For instance, the U.S. and Canadian economies witnessed a 2.14% and 1.99% increase in health expenditure between 2019 and 2020, respectively. Consequently, both the U.S. and Canada were able to provide the public with vaccines starting in December 2020, while the Japanese and Korean governments followed suit in February 2021. By December 2022, the vaccination rates per 100 people reached 247.84, 285.44, 250.19, and 197.37 for Canada, Japan, Korea, and the U.S., respectively. These vaccination efforts led to a reduction in fatality rates to 1.1%, 0.2%, 0.1%, and 1.1% for the respective countries.

<Insert Table 1 around here>

Governmental health policies are formulated with the aim of anticipating the future course of a pandemic. The effectiveness of governmental responses to the pandemic relies heavily on the accuracy of these forecasts. Accurate pandemic forecasting allows for early identification and mitigation of potential health risks, thereby preventing the spread and outbreak of the disease. Additionally, forecasting plays a crucial role in enabling healthcare systems and governments to efficiently plan and allocate resources such as medical equipment, personnel, drugs, and other necessary supplies. This ensures optimal control and mitigation of the disease's impact. For instance, if the forecasted number of future confirmed COVID-19 cases is lower than the actual ground truth, governments may face the risk of increasing fatality rates due to limited vaccine availability from suppliers. Therefore, accurate forecasting is vital for governments to make informed decisions regarding the procurement and distribution of vaccines and other essential resources.

Therefore, the primary objective of our study is to introduce an alternative methodology for forecasting COVID-19 cases that complements the forecasts generated by the standard mean and median regression methods. To achieve this goal, we leverage the benefits offered by modal regression compared to mean and median regressions. Our study focuses on forecasting the cumulative confirmed COVID-19 cases for the

four countries mentioned earlier using the modal regression approach. By utilizing this methodology, we aim to enhance the accuracy and reliability of COVID-19 forecasts, providing a valuable addition to the existing forecasting methods based on mean and median regressions.

A considerable body of literature has been dedicated to empirically analyzing the COVID-19 trend by applying various classical forecasting methods. Studies such as Boccaletti, Ditto, Mindlin, and Atangana (2020); Almeshal, Almazrouee, Alenizi, and Alhajeri (2020); Vespignani, Tian, Dye, Lloyd-Smith, Eggo, Shrestha, Scarpino, Gutierrez, Kraemer, Wu et al. (2020); Chan, Chu, Zhang, and Nadarajah (2021); Gning, Ndour, and Tchuenche (2022) have focused on estimating the strain on medical services, understanding epidemiological patterns, and providing policymakers with comprehensive information to formulate effective policies. Furthermore, Musulin, Baressi Šegota, Štifanić, Lorencin, Anđelić, Šušteršič, Blagojević, Filipović, Ćabov, and Markova-Car (2021) have conducted a review of the application of standard regression methods in various AI-based COVID-19 applications. However, it should be noted that conditional mean- or median-based forecasts can be significantly influenced by outliers or heavy-tailed noise present in the data (see Chen, Genovese, Tibshirani, and Wasserman, 2016; Zhou and Huang, 2016; Xiang and Yao, 2022, for examples). These limitations highlight the need for alternative forecasting approaches that can mitigate the impact of such data irregularities.

Modal regression is a valuable alternative to standard regression methods when forecasting random processes that contain outliers and/or exhibit heavy-tailed noise distributions. The literature on modal regression has demonstrated its advantages over other forecasting techniques. Sasaki, Sakai, and Kanamori (2020) recognize that estimating the conditional mode is more robust than estimating the conditional mean or median, particularly when dealing with wide-ranging noise. Xiang and Yao (2022) provide an intuitive location estimator for skewed data, highlighting the superiority of modal regression in such cases. Furthermore, Yao and Li (2014) introduce modal linear regression, exploring its application to high-dimensional data and analyzing its asymptotic properties without assuming a symmetric error density function. Yu, Zhu, Shi, and Ai (2020) propose a robust estimation procedure for partial functional linear regression using modal regression, specifically designed to handle outliers and heavy-tailed error distributions. Xiang and Yao (2022) also propose a novel nonparametric statistical learning tool based on modal regression, serving as a complementary approach to standard mean and median regressions. Overall, the literature highlights the advantages of modal regression in addressing the challenges posed by outliers, heavy-tailed noise, and skewed data, providing a robust and flexible forecasting methodology.

Despite recent advancements in modal regression, its application to COVID-19 data has been limited. The COVID-19 pandemic exhibits exponential growth, a wide range of governmental responses, and the

emergence of unexpected virus variants. These factors introduce unexpected noise and outliers, making COVID-19 data an excellent opportunity to explore the capabilities of modal regression. While Ullah, Wang, and Yao (2022) have conducted preliminary investigations applying modal regression to examine the interrelationship between COVID-19 cases and deaths in the U.S., there is still scope for further exploration using modal regression. In the current study, we utilize modal regression for forecasting COVID-19 data by employing specific time-series models. We then compare the results with those obtained using mean and median regressions, as highlighted in previous works (e.g., Musulin et al., 2021).

The current study contributes to the existing literature in two significant ways. First, we introduce the coverage quantile function (CQF) as a metric to evaluate the performance of modal regression. While root-mean squared error and mean absolute error are commonly used objectives for optimizing mean and median regressions respectively, we utilize CQF as the objective for the modal regression. This approach provides a clearer understanding of the role and effectiveness of modal regression in forecasting. Second, we specify an autoregressive model to capture the serial correlation present in COVID-19 data for the four countries mentioned in Table 1. We then apply modal regression to generate forecasts and compare them with forecasts obtained using mean and median regressions. Our analysis reveals that the modal regression outperforms the mean and median regressions in forecasting outliers. This finding underscores the superior performance of modal regression in handling the unique characteristics and challenges of COVID-19 data. Overall, this study's contributions lie in the introduction of CQF as a novel evaluation metric for modal regression and the empirical demonstration of its superior forecasting capabilities compared to mean and median regressions, particularly when dealing with outliers.

The methodology employed in our research involves a simulation approach. The implementation of the modal regression method relies on estimating the conditional density function, which is highly sensitive to factors such as the selection of bandwidth or the shape of the density function, as pointed out by Ullah et al. (2022). Consequently, the valuable theoretical results regarding modal regression are often challenging to validate using empirical data due to the presence of irregular data patterns. To address this challenge, we adopt an extensive simulation approach that allows us to examine the characteristics of modal regression using finite samples. We conduct Monte Carlo simulations using both cross-sectional and time-series data to evaluate the performance of mean, median, and modal regressions. Additionally, we compare the performance of different bandwidths utilized in the modal regression estimation. Furthermore, we apply the modal regression method to forecast the cumulative confirmed COVID-19 cases for the four countries mentioned earlier. Through this empirical application, we demonstrate that the modal regression-based forecast achieves a superior CQF compared to other forecasting methods. By combining simulation studies and

empirical analysis, we are able to assess the performance of modal regression under various scenarios, investigate the impact of different bandwidth choices, and showcase the advantages of modal regression in forecasting COVID-19 cases.

The structure of this study is organized as follows. In Section 2, we present a comprehensive review of the relevant literature related to the subject of this study, highlighting the motivation behind our research. Section 3 focuses on formalizing the problem of modal regression. We propose the CQF metric and provide an overview of existing modal regression methods. Simulation results are presented in Section 4, where we conduct various simulations to evaluate the performance of mean, median, and modal regressions. Section 5 is dedicated to the empirical analysis applied to COVID-19 data. We apply the modal regression method to forecast the cumulative confirmed COVID-19 cases for the four countries mentioned earlier and compare the results with other forecasting approaches. Finally, in Section 6, we provide concluding remarks summarizing the key findings of our study and discuss the implications and potential future directions of research in this field.

2 Literature Review and Motivation

There have been numerous studies focusing on analyzing and predicting the trends of COVID-19. In this section, we provide a brief overview of some of the methodologies employed in these studies.

One common approach is the development of empirical prediction models using machine learning methods. For example, Car, Baressi Šegota, Anđelić, Lorencin, and Mrzljak (2020) train a multilayer perceptron (MLP) artificial neural network to create a global model for forecasting the maximum number of patients across various locations over time. Similarly, Mollalo, Rivera, and Vahedi (2020) utilize MLP to forecast the cumulative COVID-19 incidence rates specifically for the United States. Chakraborty and Ghosh (2020) propose a hybrid approach that combines integrated autoregressive moving average models with wavelet-based forecasting models to predict the number of daily confirmed cases in the short term. Other prediction models for confirmed cases include the gradient boosting regression model, the generalized waring regression model, and various other machine learning approaches (see also Gumaei, Al-Rakhami, Al Rahhal, Albogamy, Al Maghayreh, and AlSalman, 2021; Gning et al., 2022, for more examples using the machine learning methods). These studies highlight the versatility of machine learning methods in capturing the complex dynamics of COVID-19 data and providing accurate predictions. By leveraging various machine learning algorithms, researchers have made significant strides in understanding and forecasting the spread of the virus.

In addition to machine learning methods, evolutionary computing algorithms have also been employed in developing epidemiology models that capture biological evolution through processes such as reproduction, mutation, recombination, and selection. For instance, Salgotra, Gandomi, and Gandomi (2020a) utilize gene expression programming (GEP) based on evolutionary data analysis to specify a model for the potential impact of the COVID-19 virus on the 15 most affected countries. Similarly, in another study by Salgotra, Gandomi, and Gandomi (2020b) a robust and reliable variant of the GEP method is developed to model the confirmed cases and deaths caused by COVID-19 in India. Other examples include the work by Yousefpour, Jahanshahi, and Bekiros (2020), who propose an effective and efficient multi-objective genetic algorithm to design government strategies for addressing the disease. Zivkovic, Bacanin, Djordjevic, Antonijevic, Strumberger, Rashid et al. (2021) employ a hybrid model combining adaptive neuro-fuzzy inference system and an enhanced genetic algorithm to predict the number of confirmed cases in China. These studies demonstrate the application of evolutionary computing algorithms in modeling the dynamics of the COVID-19 pandemic, providing valuable insights and predictions. By incorporating evolutionary principles, these approaches offer unique perspectives and potential for optimizing strategies to mitigate the impact of the virus.

Several studies have focused on analyzing the COVID-19 trend from an economic perspective and assessing its impact on the economy. These studies provide valuable insights into various aspects of the pandemic's economic implications. For example, Almeshal et al. (2020) investigate the effectiveness of non-pharmaceutical intervention measures in forecasting the size of the COVID-19 pandemic in Kuwait. They employ deterministic and stochastic modeling approaches to estimate the scale of confirmed COVID-19 cases and identify the ending phase of the pandemic. Their findings highlight the efficacy of non-pharmaceutical interventions, particularly when infection rates and personal contact patterns change over time. Other studies examine specific economic impacts of COVID-19. Ajide, Ibrahim, and Alimi (2020) analyze the impact of lockdown policy implementation on confirmed COVID-19 cases in Nigeria. Azimli (2020) investigate the impact of COVID-19 on the degree and dependence structure of risky asset returns in the U.S. Béland, Brodeur, and Wright (2023), Gupta, Montenovo, Nguyen, Lozano-Rojas, Schmutte, Simon, Weinberg, and Wing (2023), and Rojas, Jiang, Montenovo, Simon, Weinberg, and Wing (2020) examine the effects of COVID-19 on the labor market. Furthermore, the impact of COVID-19 on mental health and well-being has been explored by Lu, Nie, and Qian (2021), Hamermesh (2020), Béland, Brodeur, Mikola, and Wright (2022), and Tubadji, Boy, and Webber (2020), while Olmstead and Tertilt (2020) delves into the detailed examination of the impact of COVID-19 on gender inequality. Studies by Andrée (2020), He, Pan, and Tanaka (2020), Brodeur, Cook, and Wright (2021a), and Almond, Du, and Zhang (2020) investigate the

environment effects of COVID-19. These studies provide valuable insights into the multifaceted economic consequences of COVID-19 and the corresponding governmental responses. They shed light on the impacts on sectors such as labor markets, mental health, gender equality, and the environment. For a comprehensive review of the economic consequences of COVID-19 and governmental responses, Brodeur et al. (2021a) provide a recent survey.

Despite the extensive research conducted on COVID-19 and its analysis, there is variation in the forecasts generated, and they may not be directly applicable to forecasting economic activities. The existing literature often predicts the trend of COVID-19 using mean and median regressions. For example, Rojas et al. (2020) and Hamermesh (2020) employ mean regression to forecast the impact of COVID-19, while Lu et al. (2021) delve deeper into mean-based forecasts using median regression. Additionally, studies such as Béland et al. (2022), Gupta et al. (2023), Tubadji et al. (2020), and He et al. (2020) apply the difference-in-difference approach to evaluate COVID-19 policies. However, forecasting the peak of the pandemic could be more relevant when it comes to forecasting the economic environment affected by the pandemic. Economic activities before and after the peak are likely to differ significantly, making it important to accurately forecast the peak itself. Mean and median regressions may not be suitable for this purpose, as they assume the central tendency of the conditional distribution through mean and median estimations, respectively. Moreover, the mean regression is most efficient when the conditional distribution is Gaussian or sub-Gaussian, while the median regression becomes a robust estimator when the distribution is light-tailed. Unless the distribution of confirmed cases is unimodal and symmetric, mean and median regressions struggle to capture the most likely value of the conditional distributionâĂŤa challenging characteristic often observed in real-world data. Real-world data is more likely to exhibit multimodal, skewed, or fat-tailed distributions. Studies by Krief (2017) and Ullah, Wang, and Yao (2021) have demonstrated that mean and median regressions lose their robustness and/or efficiency when time series datasets contain multiple outliers and/or skewed distributions.

This aspect serves as motivation to forecast the peak by estimating the mode of the conditional distribution. To achieve this, we utilize the modal regression, which is specifically designed to estimate the mode of a conditional distribution. In addition to estimating the same quantities as the mean and median regressions under the assumption of a unimodal and symmetric conditional distribution, the modal regression offers several additional properties. First, the modal regression is more robust to outliers compared to the mean and median estimators since it utilizes the mode as a representation of the central tendency of the conditional distribution. Second, the modal regression can yield narrower forecasting intervals compared to other estimations. This is because the interval around the conditional mode contains more observations than those around the conditional mean and/or median for the same interval size. Finally, in the case of data drawn

from a multimodal conditional distribution, the modal regression captures a different central tendency than the mean and/or median. This enables the exploration of different aspects of the conditional distribution. In this study, we apply the modal regression to forecast confirmed COVID-19 cases in Canada, Japan, Korea, and the U.S. Subsequently, we compare these forecasts with those obtained through mean and median regressions to assess the performance and advantages of the modal regression approach.

3 Method of Modal Regression

In this section, we will delve into the methodology of the modal regression and the models used for forecasting. Additionally, we will provide a comprehensive explanation of the criterion used to evaluate the forecasts generated by the modal regression.

3.1 Modal Regression

We first discuss the limitations of the mean regression for forecasting and compare its characteristics with those of the modal regression. To begin, let $\mathcal{X} \subset \mathbb{R}^d$ and $\mathcal{Y} \subset \mathbb{R}$ represent the spaces of regressors and the dependent variable, respectively. We consider a dataset $\mathcal{S} = (x_t, Y_t) \in \mathcal{X} \times \mathcal{Y} : t = 1, 2, \ldots, n$ consisting of independent and identically distributed random samples.[1] Given this setup, we define the conditional mode function $f(x)$ as the mode of the conditional probability density function $p_{Y|X}(\cdot)$, representing the density of $Y \in \mathcal{Y}$ conditioned on $X \in \mathcal{X}$. Mathematically, we have:

$$f(x) := \text{mode}(Y|X = x) := \arg\max_y p_{Y|X}(y|X = x).$$

Additionally, we introduce the variable U, defined as the difference between Y and $f(X)$, i.e., $U := Y - f(X)$. Under the assumption that $p_{U|X}(\cdot|X = x)$ is continuous and bounded for any $X = x \in \mathcal{X}$, the conditional mode of U given $X = x$ is denoted as $\text{mode}(U|X = x)$, which satisfies $\arg\max_y p_{U|X}(y|X = x) = 0$. It is important to note that we assume the conditional density function $p_{Y|X}(\cdot|X = x)$ has a unique maximum with probability 1, ensuring that $f(x)$ is well-defined for any $x \in \mathcal{X}$. This assumption guarantees the existence and uniqueness of the global mode of $f(\cdot)$.[2] Furthermore, we note that maximizing the conditional density $p_{Y|X}(\cdot|X = x)$ is equivalent to maximizing the joint density $p_{X,Y}(X = x, Y = \cdot)$

[1] It is important to note that COVID-19 data are non-stationary and typically exhibit serial correlation in the error terms, which violates the assumption of independence and identical distribution. We will address this issue by specifying a model for serial correlation later in the study.

[2] This type of conditional mode function is known as the unimodal regression function (e.g., Chen, 2018), while Chen et al. (2016) relaxes the uniqueness condition in a nonparametric model regression context. In our study, we focus on the unimodal case.

since $p(y|x) = p(x,y)/p(x)$ for a fixed $x \in \mathcal{X}$. Therefore, the conditional mode can also be expressed as $\arg\max_y p(y,x)$, indicating that the estimation of the conditional mode is related to estimating the density function of the random variables.

We explore this aspect by representing the conditional mode by a parametric model. Specifically, we let $\mathcal{M} := \{m(X,\theta) : \theta \in \Theta\}$ be a parametric model for the conditional mode such that for a unique $\theta_* \in \Theta$, mode$(Y|X) = m(X,\theta_*)$, where Θ is a compact parameter space in $\mathbb{R}^p$, and for each $\theta \in \Theta$, $m(\cdot,\theta)$ is a measurable function. Given this parametric model assumption, we estimate θ_* by maximizing the kernel based objective function:

$$Q_{n,h}(\cdot) := \frac{1}{n}\sum_{t=1}^{n}\phi_h\left(Y_t - m(X_t,\cdot)\right),$$

where for each $u \in \mathbb{R}$, $\phi_h(u) = h^{-1}\phi(u/h)$ such that $\phi(\cdot)$ is a kernel density function that is symmetric around 0 and $\int \phi(u)du = 1$, and h is the bandwidth. A range of commonly used kernel functions include Gaussian, Epanechnikov, uniform, triangular and so on. For the remainder of the paper, we assume that $\phi(\cdot)$ is the standard normal density function for simplicity. By maximizing the objective function $Q_{n,h}(\cdot)$, we can estimate the value of θ_* that corresponds to the conditional mode. This approach allows us to represent the conditional mode using a parametric model and estimate the associated parameters.

The maximization of $Q_{n,h}(\cdot)$ requires a numerical optimization procedure since there is no closed-form expression for its maximum. Various numerical optimization algorithms can be employed to maximize $Q_{n,h}(\cdot)$, such as the Modal Expectation and Maximization (MEM) algorithm, Newton-type algorithms, and mean-shift algorithms (see Yao and Li, 2014; Khardani and Yao, 2017; Chen et al., 2016, respectively). Among these optimization methods, the MEM algorithm has shown robust performance, as demonstrated in the simulations outlined in Section 4. Therefore, for our empirical applications, we utilize the MEM algorithm as the chosen numerical optimization procedure to maximize $Q_{n,h}(\cdot)$ and estimate the parameters associated with the conditional mode.

The MEM algorithm proposed by Li, Ray, and Lindsay (2007) extends the EM algorithm (Dempster, Laird, and Rubin, 1977) to the context of modal regression. While the EM algorithm assumes the presence of latent variables in the likelihood function, the MEM algorithm considers their presence in the density function and estimates the unknown parameters using the E- and M-steps. Specifically, the E-step involves computing the weight of each observation. Given an initial parameter $\theta^{(0)}$, for each observation $(Y_t, X_t')'$, we calculate

$$\pi(t|\theta^{(0)}) := \frac{\phi_h(Y_t - m(X_t;\theta^{(0)}))}{\sum_{i=1}^{n}\phi_h(Y_t - m(X_t;\theta^{(0)}))},$$

where $\phi_h(\cdot)$ is the kernel density function. Next, the M-step maximizes the objective function:

$$\theta^{(1)} := \arg\max_{\theta\in\Theta} \sum_{t=1}^{n} \left\{ \pi(t|\theta^{(0)}) \log \phi_h \left(Y_t - m(X_t;\theta) \right) \right\}.$$

Using the updated parameter $\theta^{(1)}$, we compute $\pi(t|\theta^{(1)})$ for each t and repeat the maximization process, replacing $\theta^{(0)}$ in the objective function. We iterate the E- and M-steps until the maximizing parameter converges. Denoting the converged parameter as $\widehat{\theta}_n$, it maximizes the objective function $Q_{n,h}(\cdot)$ since each iteration progressively maximizes $Q_{n,h}(\cdot)$. In the Appendix, we provide a proof that for any positive integer k, $Q_{n,h}(\theta^{(k+1)}) - Q_{n,h}(\theta^{(k)}) \geq 0$. Therefore, as k tends to infinity, the maximum of $Q_{n,h}(\cdot)$ is reached. This proof remains valid even when $m(X_t;\cdot)$ is nonlinear, thereby generalizing the proof presented by Yao and Li (2014) that assumes a linear model for the conditional mode.

The MEM algorithm relies on estimating the objective function using kernel density function estimation, which is influenced by the choice of bandwidth h. However, as highlighted by Ullah et al. (2022) and confirmed by our Monte Carlo simulations in Section 4, the convergence of $\widehat{\theta}_n$ to the unknown true parameter critically depends on the selection of the bandwidth. Among various bandwidth selection methods, the bandwidth suggested by Sheather and Jones (1991), referred to as SJ, generally produces robust estimation results along with other bandwidths such as those selected by Scott's (1979) and Silverman's (1986) rule of thumb. The SJ's bandwidth is given as follows: Suppose $z_1, z_2, \ldots, z_n$ represents the sample points of a random variable Z,

$$\text{SJ's bandwidth: } h_n^{SJ} := \left(\frac{\int k^2(u)du}{n\widehat{\sigma}_n^4 \int \left[\widehat{f}_n''(u)\right]^2 du} \right)^{\frac{1}{5}},$$

where $\widehat{\sigma}_n$ is the estimated standard deviation using the sample points, $k(\cdot)$ is a kernel function used to weigh the sample points, and $\widehat{f}_n''(\cdot) := \frac{1}{nh_0^3}\sum_{t=1}^{n} L''\left(\frac{(\cdot)-z_t}{h_0}\right)$ estimates $f''(\cdot)$, the second derivative of the density function $f(\cdot)$ of Z. Here, h_0 is a bandwidth and $L(\cdot)$ is the kernel function used to estimate $f(\cdot)$. SJ suggest using a simple rule of thumb for h_0. In addition to SJ's bandwidth, two other commonly used bandwidths are as follows:

$$\text{Scott's bandwidth: } h_n^{SC} := 1.06\widehat{\sigma}_n n^{-1/5}, \quad \text{and}$$
$$\text{Silverman's bandwidth: } h_n^{SV} := 0.9\min[\widehat{\sigma}_n, IQR_n/1.34]n^{-1/5},$$

where IQR_n represents the interquartile range of the sample points, which is the distance between the second and third quartiles.

When applying the MEM algorithm, we combine it with least squares estimation to first estimate the density function. Here is the procedure we follow when using Scott's bandwidth as an example: first, we begin by estimating the standard deviation, denoted as $\widehat{\sigma}_n^{(1)}$, using the residuals obtained from the least squares estimation. Next, we apply the MEM algorithm to the density function estimated using Scott's bandwidth, using $\widehat{\sigma}_n^{(1)}$, and obtain the first-step MEM estimator, denoted as $\theta^{(1)}$. Using $\theta^{(1)}$, we compute different residuals to estimate the standard deviation, denoted as $\widehat{\sigma}_n^{(2)}$, and estimate the density function using $\widehat{\sigma}_n^{(2)}$. We then maximize this new density function and obtain the second-step MEM estimator, denoted as $\theta^{(2)}$. We continue this iterative process, estimating $\widehat{\sigma}_n^{(k)}$ and obtaining the k-th step MEM estimator $\theta^{(k)}$, until we reach convergence and obtain $\widehat{\theta}_n$. We propose estimating $\widehat{\sigma}_n^{(1)}$ using least squares estimation because it is not straightforward to estimate $\widehat{\sigma}_n$ directly using the MEM algorithm when the data are nonstationary. For such cases, it is useful to estimate the conditional mean first, as demonstrated by the simulation in Section 4.2 using a unit-root process.

The main objective of modal regression differs from that of mean and median regressions. While the mean squared error (MSE) and mean absolute error (MAE) are typically used as target metrics for optimizing mean and median regressions, respectively, these metrics do not align with the objective of the conditional mode function (see, e.g., Buhai, 2005; Porter, 2015). Therefore, for modal regression, we require a different target metric. Given that the conditional mode reflects the density in the vicinity of $f(x)$ directly, a natural objective metric can be defined based on the number of observations around the estimator. In this context, the CQF can serve as an appropriate objective metric for modal regression. Specifically, for a given $\tau \in (0, 1)$, if κ is the quantity satisfying the equality

$$\mathbb{E}[\mathbb{I}(|Y - g(X)| \leq \kappa)] = \tau,$$

where $\mathbb{I}(\cdot)$ is the indicator function and $g(X)$ is a quantity defined by X, we can characterize the behavior of the conditional mode using κ. Intuitively, as κ becomes smaller, $g(X)$ should approach the conditional mode $f(X)$, indicating that for a fixed τ, we can estimate κ to measure the extent to which the conditional density of $Y|X$ concentrates around $g(X)$. In light of this, we define the sample analog for the CQF as:

$$\frac{1}{n}\sum_{i=1}^{n} \mathbb{I}(|Y_t - \widehat{g}_n(X_t)| \leq \kappa) = \tau,$$

where $\widehat{g}_n(X_t)$ is a generic estimator. This equation allows us to determine κ that satisfies the equality, providing a measure of how well the estimator captures the concentration of the conditional density around

$g(X)$. For the empirical applications discussed in Section 5, we set $\tau = 0.50$, meaning that the interval around $g(X_t)$ with a distance of 2κ covers half of the observations in the dataset. When $\widehat{g}_n(X_t)$ estimates the conditional mode, we can expect the interval characterized by κ to be narrower compared to those characterized by the conditional mean or median.[3]

3.2 Extension of the Modal Regression

In this section, we extend the application of modal regression to time-series data. This is necessary because the data assumption made in the previous section does not account for the presence of serial correlation in the cumulative confirmed COVID-19 cases. To address this issue, we introduce time-series models that explicitly capture the serial correlation structure.

For the purpose of this section, we focus on specifying models for trend and serial correlation separately. The first-step procedure involves modeling the trend component, while the second-step procedure focuses on modeling the unit-root process, which captures the serial correlation. The first-step procedure is necessary because COVID-19 data typically do not follow a linear deterministic time trend process. Instead, the mode of each observation is represented as a function of the time index. The empirical analysis in Section 5.1 demonstrates that the nonlinearity of the COVID-19 trend is more complex than a simple linear trend process. The second-step procedure aims to transform the COVID-19 data into a stationary process with serial correlation. By accounting for the serial correlation, we can capture the temporal dependencies present in the data and ensure that the modal regression analysis is applicable. By separately specifying models for trend and serial correlation, we can effectively capture the characteristics of time-series data and enhance the accuracy of the modal regression analysis for COVID-19 data.

In the first-step procedure, we focus on specifying the nonlinear trend component. We employ three estimation methods, the first of which is the B-spline modal regression (BMR) proposed by Yu et al. (2020). To implement the BMR, we utilize B-splines, which are a type of basis functions. We define ξ as the knots of the expected B-spline, which partitions the unit interval $[0, 1]$. Each $t_i \in [0, 1]$ corresponds to a knot, and we construct the linear spline space using $(k - \ell)$ B-spline basis functions of order ℓ. Here, the unit interval represents the time index space, obtained by dividing time by the sample size n, i.e.,$\{\frac{1}{n}, \frac{2}{n}, \ldots, \frac{n-1}{n}, \frac{n}{n}\}$.

[3]It is also possible to interpret this association in the opposite manner: for a fixed κ, if $g(X) = f(X)$, the interval around the conditional mode can cover more samples than any other quantity $g(X) \neq f(X)$. This implies that τ increases as $g(X)$ approaches $f(X)$.

The basis functions are defined as follows: for $i = 0, 1, \ldots, k - \ell - 1$,

$$B_{i,0}(\tau) := \begin{cases} 1, & \text{if } t_i \leq \tau < t_{i+1} \\ 0, & \text{otherwise,} \end{cases}$$

and

$$B_{i,\ell}(\tau) := \frac{x - t_i}{t_{i+\ell} - t_i} B_{i,i-\ell}(\tau) + \frac{t_{i+\ell+1} - x}{t_{i+\ell+1} - t_{i+1}} B_{i+1,\ell-1}(\tau),$$

where $B_{i,\ell}(\cdot)$ represents the i-th basis function of order ℓ. For simplicity, we denote $B_{i,\ell}(\cdot)$ as $B_i(\cdot)$, and the B-spline basis function is denoted as $B(\cdot) = B_0(\cdot), B_1(\cdot), \ldots, B_{(k-\ell-1)}(\cdot)$. Under this setup, we assume that the conditional mode is a linear function of $B(\tau)$, i.e., $m(\tau, \theta) = \theta' B(\tau)$, and estimate the parameter vector $\theta = (\theta_0, \ldots, \theta_{k-\ell-1*})'$ using modal regression. It is important to note that the choice of (ξ, ℓ) has a deterministic impact on the shape of the spline function. The selection of ξ determines the positioning of control points, while ℓ determines the number of coefficients in each piece of the piecewise polynomial representation.

Different types of B-splines can be defined by choosing (ξ, ℓ) in different ways. Here are a few examples of well-known B-splines: first, for the nonperiodic B-spline, the first and last m knots are fixed at 0 and 1, respectively, where $2m < k + 1$. For instance, if we choose $\xi = 0, 0, 0, 0.3, 0.6, 1, 1, 1$, it corresponds to the nonperiodic B-spline knots. Second, the uniform B-spline assumes equally spaced knots. For example, if we select $\xi = 0, 0.25, 0.5, 0.75, 1$, it represents the uniform B-spline knots. Third, Bezier knot lets $k = 1$, so that the knots are set as $\xi = 0, 1$.

The choice of (ξ, ℓ) is typically determined empirically based on the characteristics of the data. For example, if the data exhibit a curve resembling a quadratic function, the nonperiodic B-spline can be employed by setting the first and last $\ell + 1$ knots to 0 and 1, respectively, and placing ℓ knots in the middle. Yu et al. (2020) demonstrate that the BMR is robust against outliers or heavy-tailed error distributions. Moreover, they show that BMR performs no worse than least squares estimation when the errors are normally distributed.

Second, the local polynomial modal regression (LPMR) method, as examined by Xiang and Yao (2022), can be employed as a second estimation method to estimate the modal function. The LPMR involves applying a p-th order Taylor expansion for the conditional mode around a reference value of $\tau \in [0, 1]$, specifically

$\frac{t}{n}$, to approximate $f(\tau)$. This approximation can be expressed as:

$$f(\tau) \approx \sum_{i=0}^{p} \frac{f^{(i)}\left(\frac{t}{n}\right)}{i!}\left(\tau - \frac{t}{n}\right)^{i} = \sum_{i=0}^{p} \theta_{i*}\left(\tau - \frac{t}{n}\right)^{i},$$

where $\theta_{i*} := f^{(i)}\left(\frac{t}{n}\right)/i!$ and $f^{(i)}(\cdot)$ represents the i-th order derivative of $f(\cdot)$. Similar to the B-spline modal regression, the parameter vector θ_* can be estimated by applying modal regression. In the LPMR method, the optimal order p can be chosen by minimizing the CQF with respect to the degree of the polynomial. Xiang and Yao (2022) demonstrate through simulation that the LPMR method complements the conventional nonparametric mean and median regressions, particularly in the presence of outliers. Furthermore, they show that LPMR exhibits better prediction performance for skewed data compared to mean and median regressions.

Lastly, we apply the linear modal regression (MR) using the approach described in Yao and Li (2014). This method assumes a linear model for $f(\frac{t}{n})$ as $m(\frac{t}{n}, \theta_*) = \theta_0 + \theta_{1*}\frac{t}{n}$, where $\theta_* := (\theta_0, \theta_{1*})'$ is estimated through modal regression. It is important to note that this linear model is not a suitable representation for COVID-19 data. However, we utilize it as a benchmark model to contrast its linearity against a process with a linear trend.

Additionally, Zhou and Huang (2019) propose the mean shift modal regression (MSMR) method for nonparametric trend prediction. However, we have found that the forecasting error of MSMR is greater than that of the first two methods (BMR and LPMR). As a result, we focus on the BMR, LPMR, and MR methods to predict the trend in our analysis.

As the second step in specifying a model for correlation, we apply the autoregressive (AR) model. The AR model is defined as follows:

$$Y_t = \alpha_* + \sum_{i=1}^{\ell} \beta_{i*} Y_{t-i} + U_t, \tag{1}$$

where α_* and β_{i*} are the parameters to be estimated, and U_t represents the error term. We distinguish between two versions of the AR model based on the type of error term. First, we have the mean autoregressive (MEAR) process, which assumes that U_t follows a white noise process with zero mean and constant variance. This is the conventional AR process. On the other hand, for modal regression, we assume that U_t is a white noise process with zero conditional mode given $\mathcal{F}_t$, where $\mathcal{F}_t$ is the sigma-algebra generated by Y_{t-1}, Y_{t-2}, and so on. We refer to this version as the modal autoregressive (MAR) process. If the series Y_t is not stationary, we apply differencing to obtain a stationary process. In this case, we replace Y_t and Y_{t-i} in (1) with ΔY_t and ΔY_{t-i}, respectively, and estimate the parameters $\theta_* := (\alpha_*, \beta_{1*}, \ldots, \beta_{\ell*})'$ using modal

regression. If ΔY_t is still nonstationary, we repeat the differencing process until we obtain a stationary process. The MAR model for a differenced process of order d can be expressed as:

$$\Delta^d Y_t \ = \alpha_* + \sum_{i=1}^{\ell} \beta_{i*} \Delta^d Y_{t-i} + U_t.$$

The lag order ℓ can be determined by applying the Bayesian information criterion (BIC), commonly used for estimating the MEAR process. Since U_t is determined by the conditional distribution of $\Delta^d Y_t$ given $\Delta^d Y_{t-i}$ $(i = 1, 2, \ldots)$, the BIC can effectively assist in estimating the lag order of the MAR process.

4 Evaluation of the Modal Regression by Simulation

n this section, we perform Monte Carlo simulations to examine the application of modal regression and evaluate its effectiveness compared to other estimation methods. We consider two types of data generating processes (DGPs): cross-sectional data and time-series data. Through these Monte Carlo simulations, we aim to gain a comprehensive understanding of the capabilities and limitations of modal regression, particularly in comparison to alternative estimation approaches, in both cross-sectional and time-series settings.

4.1 Simulation Using Cross-Sectional Data

We demonstrate the application of modal regression by comparing it with mean and median regressions. We start by generating a set of identically and independently distributed (IID) observations $\{(X_t, Y_t) : t = 1, \ldots, n\}$ according to the following formula: $Y_t = \alpha_* + \beta_* X_t + U_t$. In this case, we set $\alpha_* = 0$, $\beta_* = 2$, $X_t \sim_{iid} U[0, 1]$, and $U_t \sim_{iid} 0.5N(-2, 3^2) + 0.5N(2, 1^2)$, ensuring that X_t and U_t are independent. We refer to this data generating process as DGP1. The left panel of Figure 1 displays the density function of U_t, where we can observe that the expected value $\mathbb{E}(U_t) = 0$, the median $\text{median}(U_t) = 1$, and the mode $\text{mode}(U_t) = 2$. As a result, the following relationships hold:

$$\mathbb{E}\left(Y_t \mid X_t\right) = \alpha_{1*} + \beta_{1*} X_t = 2X_t, \quad \text{median}\left(Y_t \mid X_t\right) = \alpha_{2*} + \beta_{2*} X_t = 1 + 2X_t, \quad \text{and}$$

$$\text{mode}\left(Y_t \mid X_t\right) = \alpha_{3*} + \beta_{3*} X_t = 2 + 2X_t.$$

This implies that the conditional mean, median, and mode functions are associated with different parameter values. The right panel of Figure 2 illustrates the three different functions, represented by the blue, orange, and red lines, respectively. Additionally, 200 observations randomly drawn from DGP1 are shown. We can

observe that more observations align with the red line, indicating an asymmetric conditional distribution. The forecast band encompasses a higher concentration of observations around the conditional mode function compared to the other functions. To estimate these three functions, we utilize the mean regression (MER), linear quantile regression (LQR) with a quantile level of 0.5, and MR, respectively.

<Insert Figures 1 and 2 around here>

As highlighted by Ullah et al. (2022), the choice of bandwidth is crucial for the estimation results when using the MR method. In our simulations, we explore different bandwidth values and observe that the results are comparable when using SJ's, Scott's, and Silverman's bandwidth selection methods. Therefore, we proceed with discussing the simulation results focusing on the three density function estimations. To estimate the density function, we follow a two-step approach. First, we employ least squares estimation to obtain the conditional residuals. Then, we optimize the conditional density function using the MEM algorithm, as described in Section 3.1 of our paper. This allows us to obtain reliable estimates of the density function.

We present the simulation results in the first panel of Table 2. We conduct 1,000 independent experiments for different sample sizes ($n = 100$, 200, 300, 500, and 1,000) and report the MSEs of the estimated coefficients. The MSE provides a measure of the average squared difference between the estimated coefficients and the true coefficients across the simulation experiments.

<Insert Table 2 around here>

The simulation results can be summarized as follows:

(a) The MER, LQR, and MR methods consistently estimate the unknown parameters. As the sample size n increases, the MSEs decrease for all three methods, indicating improved estimation accuracy with larger sample sizes.

(b) The MSEs obtained by the MR methods are generally similar among the different density function estimation methods. However, a regular rank relationship can be observed among the MR methods. Specifically, the MSEs obtained using SJ's bandwidth tend to be smaller compared to the other methods. On the other hand, there is no consistent rank relationship between the MSEs obtained using Scott's and Silverman's bandwidths. This suggests that SJ's bandwidth tends to provide more accurate estimation results in terms of MSE for the MR method, while the relative performance of Scott's and Silverman's bandwidths may vary depending on the specific data and model conditions.

(c) We also examine the distribution of the estimated coefficients. The upper panels of Figure 3 display the estimated probability density functions of $\widehat{\alpha}_n$ and $\widehat{\beta}_n$ obtained by the MER method using SJ's

bandwidth. It can be observed that the empirical distributions of the estimated coefficients are close to bell-shaped distributions. This indicates that the estimated coefficients tend to be centered around their true values, and the variability around the mean is relatively symmetric. □

<Insert Figure 3 around here>

Using DGP1, we verify that the MEM algorithm consistently estimates the conditional mode, while the MER and LQR estimations estimate the conditional mean and median, respectively.

We further explore the modal regression by considering a different DGP condition, DGP2. In DGP2, we assume another distribution for the error term instead of the mixture normal distribution. Similar to DGP1, we have $Y_t = \alpha_* + \beta_* X_t + U_t$, where $\alpha_* = 0$, $\beta_* = 1$, $X_t \sim_{iid} U[0,1]$, and $U_t \sim_{iid} \mathcal{X}^2_3 - 3$ with $X_t \perp U_t$, indicating that U_t follows a chi-squared distribution with three degrees of freedom shifted by three. The right panel of Figure 1 displays the density function of U_t for DGP2. We specifically examine DGP2 to investigate the performance of the modal regression when the error distribution has fat tails. The density function of U_t exhibits an extreme left fat tail due to the truncation at the border from the left, and the right tail is fatter than that of a normal distribution by construction. Consequently, we anticipate the modal regression to perform relatively poorly compared to DGP1, as more observations are required to estimate the density function accurately. It is worth noting that $\mathbb{E}(U_t) = 0$, median$(U_t) = -0.63$, and mode$(U_t) = -2$. Consequently, we have:

$$\mathbb{E}\left(Y_t \mid X_t\right) = \alpha_{4*} + \beta_{4*} X_t = X_t, \quad \text{median}\left(Y_t \mid X_t\right) = \alpha_{5*} + \beta_{5*} X_t = -0.63 + X_t, \quad \text{and}$$

$$\text{mode}\left(Y_t \mid X_t\right) = \alpha_{6*} + \beta_{6*} X_t = -2 + X_t.$$

The right panel of Figure 2 displays the three different functions along with 200 observations randomly drawn from DGP2. Similar to DGP1, we observe that more observations are distributed along the conditional mode function.

Using the observations generated from DGP2, we perform independent experiments following the same procedure as for DGP1, and the results are presented in the second panel of Table 2. The simulation results can be summarized as follows:

(a) As for DGP1, the MER, LQR, and MR methods consistently estimate the unknown parameters for DGP2. Similar to DGP1, we observe that the MSEs decrease as the sample size n increases for all three estimation methods. While the MSEs obtained by the MR methods are generally larger than those obtained by the MER and LQR methods, we can confirm that the MR methods provide

consistent MR estimators. For brevity, we do not report the detailed simulation results, but it is worth noting that as the sample size increases to 2,000, the MR estimators become very close to the true unknown parameters.

(b) When comparing the MSEs obtained by the MR methods for DGP2, we find that they are similar in general. However, it is consistent with the observations for DGP1 that the MSE obtained by SJ's method is overall smaller than those obtained by Scott's and Silverman's methods. This suggests that SJ's bandwidth selection method tends to yield more accurate results in terms of MSE compared to the other two methods.

(c) The lower panels of Figure 3 depict the empirical density functions of $\widehat{\alpha}_n$ and $\widehat{\beta}_n$ obtained by the MER method using SJ's bandwidth for DGP2. While the empirical distributions are not perfectly bell-shaped, we can observe that they gradually converge to normal distributions. However, this convergence is slower compared to DGP1 due to the presence of fat tails in the error distribution. The fat tails contribute to deviations from perfect normality in the empirical density functions. □

From the additional simulation using DGP2, we can observe that the modal regression effectively estimates the conditional mode. Despite the presence of fat tails in the error distribution, estimating the density function using SJ's bandwidth remains more efficient compared to the other methods. This result suggests that SJ's bandwidth selection is robust and effective in capturing the characteristics of the conditional mode, even in the presence of non-normal and fat-tailed error distributions.

In addition to the simulations presented in this study, other simulations were conducted by assuming different error distributions, and consistent results were obtained. For instance, when considering an asymmetric Beta distribution for U_t, it was observed that the parameter estimators obtained through modal regression exhibited faster convergence to the unknown parameters. This further supports the effectiveness and robustness of the modal regression method in various error distribution scenarios.

4.2 Simulation Using Non-Stationary Data

We further extend our simulation by considering serially correlated time-series data. As an extreme case, we examine the unit-root process given by:

$$Y_t = \alpha_* + \beta_* Y_{t-1} + U_t,$$

where $\alpha_* = 0$, $\beta_* = 1$, and $U_t \sim_{\text{iid}} 0.3N(-2, 3^2) + 0.2N(2, 2^2) + 0.5N(1, 1^2)$. It is important to note that $\mathbb{E}(U_t) = 0.3$, median$(U_t) = 0.75$, and mode$(U_t) = 1$. Consequently, we can derive the following

equations:

$$\mathbb{E}\left(Y_t \mid Y_{t-1}\right) = \alpha_{7*} + \beta_{7*}X_t = 0.3 + Y_{t-1}, \quad \text{median}\left(Y_t \mid Y_{t-1}\right) = \alpha_{8*} + \beta_{8*}X_t = 0.75 + Y_{t-1}, \quad \text{and}$$

$$\text{mode}\left(Y_t \mid Y_{t-1}\right) = \alpha_{9*} + \beta_{9*}X_t = 1 + Y_{t-1}.$$

We conduct simulations to examine the behavior of the estimators in terms of MSE. The experimental results are presented in Table 3, obtained by performing 1,000 independent experiments. Similar to the previous simulations, we estimate the components of the bandwidth used in the density function estimation by first estimating the conditional mean. The simulation results can be summarized as follows:

(a) For all the cases considered in our simulations, we observe a consistent decrease in MSE as the sample size n increases. This indicates that the MER, LQR, and MR methods are consistent in estimating the unknown parameters. Moreover, the decreasing trend of MSEs as n increases suggests that the modal regression is an effective estimation method, even for the unit-root process.

(b) When comparing the MSEs obtained by the MR methods, we consistently observe that the MSE obtained by SJ's method is overall smaller than those obtained by the other two methods, as we have previously observed in the cross-sectional data simulations. This suggests that SJ's method performs better in terms of MSE when estimating the density function in the modal regression framework, regardless of the data generating process.

(c) Figure 4 displays the estimated probability density functions using $\widehat{\alpha}_n$ and $\widehat{\beta}_n$ obtained by the MAR method using SJ's bandwidth. From the figure, we can observe that the empirical density functions exhibit shapes that are close to the normal distribution. However, it is important to note that a more thorough investigation is required to fully understand the influence of the unit-root process on the asymptotic distribution. In particular, since the mean and median regressions do not produce asymptotically normally distributed estimators, it becomes interesting to examine the behavior of the asymptotic distribution under the modal regression framework. Although we did not conduct a detailed analysis in this study, the empirical density functions obtained from the simulation results appear to resemble bell-shaped distributions as the sample size increases. Investigating the asymptotic distribution under the presence of a unit-root process could be a promising avenue for future research. This analysis would shed light on the behavior and properties of the estimators obtained through the modal regression, providing a more comprehensive understanding of its performance in the context of unit-root processes. □

<Insert Table 3 and Figure 4 around here>

5 Empirical Analysis

In this section, we focus on analyzing the trends of COVID-19 processes in Canada, Japan, Korea, and the U.S. using the modal regression approach. To conduct this analysis, we utilize the official data on COVID-19 provided by the Johns Hopkins University Center for Systems Science and Engineering (JHU-CSSE). This data collection incorporates information from various sources such as the WHO, national governments, and local media reports, enabling comprehensive tracking of the disease. Starting from January 22, 2020, JHU-CSSE has been updating and publishing daily data on the cumulative number of confirmed COVID-19 cases, deaths, and recoveries for each country and territory. These data sets serve as the basis for our analysis, allowing us to examine the patterns and dynamics of the COVID-19 pandemic in Canada, Japan, Korea, and the U.S. from a modal regression perspective.[4]

5.1 Forecasting the Confirmed COVID-19 Cases by Trend Fitting

Using the cumulative confirmed COVID-19 cases data from February 8, 2022, to April 8, 2022, we apply various nonlinear trend estimation methods: BMR, LPMR, and MR, in addition to the MER and LQR methods. Each country's dataset consists of 60 observations, and we split these observations into two parts. The first 50 observations are used as the training set to estimate the trends, while the remaining 10 observations serve as the test set to evaluate the performance of each method. To assess the performance of each method, we use three evaluation metrics: RMSE, MAE, and CQF. These metrics provide measures of accuracy and reliability for comparing the estimated trends across the different methods and countries.

In the empirical applications, we follow a three-step process. First, we apply min-max normalization to standardize the data. The transformed data is denoted as Y_t' and is calculated as:

$$Y_t' := \left(\frac{Y_t - Y_0}{Y^0 - Y_0} \right),$$

where $Y^0 := \max_{t=1,2,\ldots,n} Y_t$ and $Y_0 := \min_{t=1,2,\ldots,n} Y_t$. This normalization converts the large number of confirmed cases into a range between zero and one. Additionally, we adjust the time index t to be within the unit interval by rescaling it to $\frac{t}{n}$. As a result, Y_t' is readjusted to Y_τ', where $\tau = \frac{1}{n}, \frac{2}{n}, \ldots, 1$. This adjustment allows us to fit the trend of $Y_{(\cdot)}'$. In the second step, we assume that $Y_{(\cdot)}'$ follows a linear

[4]The data are available at the following URL: https://github.com/CSSEGISandData/COVID-19

trend and estimate the intercept and linear coefficient using the MER, LQR, and MR methods. We then compute the RMSE, MAE, and CQF using both the training and test sets. Finally, we consider the possibility of $Y'_{(\cdot)}$ having a nonlinear trend and estimate the trend using the BMR and LPMR methods. For the BMR method, we set the B-spline order ℓ to 3, following Yu et al. (2020), and choose 11 knots denoted as $\xi = \{0, 0, 0, 0, 0.2, 0.4, 0.6, 1, 1, 1, 1\}$. These knots are selected based on the observation that the empirical curves resemble quadratic functions. For the LPMR method, we determine the polynomial degree by minimizing the CQF. We also compute the RMSE, MAE, and CQF using the training and test sets, similar to the linear trend case.

<Insert Table 4 and Figure 5 around here>

We present the estimation and prediction results in Figure 4 and Table 4. Figure 4 shows scatter plots of all the data points considered, along with the regression lines obtained from the different regression methods. To convert the predicted values $Y'_{(\cdot)}$ back to the original scale, we use the formula $\widehat{Y}_{(\cdot)} := \widehat{Y}'_{(\cdot)}(Y^0 - Y_0) + Y_0$, where $\widehat{Y}'_{(\cdot)}$ represents the series predicted by each regression method. Table 4 presents the RMSE, MAE, and CQF for the four countries. Based on the results, we summarize the estimation and forecast results as follows:

(a) The MER, LQR, and MR methods demonstrate superior performance in terms of RMSE, MAE, and CQF, respectively. This finding aligns with the characteristics of these estimators and their relationship to the respective objective functions.

(b) In the training set, the modal regression methods, particularly the LPMR and BMR methods, exhibit superior performance compared to the mean and median regression methods for all four countries. In the test set, the LPMR and BMR methods continue to outperform the other regression methods for Japan and the U.S., while the MR method performs better than the other regression methods for Canada and Korea. This trend is depicted in Figure 5. Moreover, the LPMR method consistently outperforms the other modal regression methods. The optimal value of p is chosen by minimizing the CQF. Additionally, Table 4 illustrates that the LPMR method achieves lower RMSE and MAE values compared to the BMR method in most cases. In terms of CQF, both the LPMR and BMR methods offer competitive performance.

(c) Although estimating a linear modal trend is straightforward, its performance, as measured by the CQF, is consistently surpassed by the BMR and LPMR methods. This indicates that the COVID-19 confirmed cases in the four countries do not conform to a linear trend.

(d) For the test sets of Korea and the U.S., the forecast lines generated by the MR method are closer to

the actual values compared to those produced by the MER and LQR methods. This indicates that the MR method performs better in forecasting the highest and lowest values of confirmed cases in Korea and the U.S., respectively. It implies that if the Korean government relies solely on mean and median regression perspectives to formulate health policies, there is a risk of healthcare systems being overwhelmed by the actual number of confirmed cases surpassing the forecasts based on mean and median regressions. Similarly, implementing health policies in the U.S. without considering the conditional mode forecast may lead to the misallocation of financial and human resources. □

By comparing the different regression methods, we find that the modal regression outperforms the mean and median regressions in both the training and test sets for all four countries, especially in terms of the CQF. This observation confirms that the modal regression methods, which emphasize the conditional mode, yield narrower forecast intervals compared to traditional approaches that primarily focus on the characteristics of the conditional mean and median to achieve better RMSE or MAE scores, respectively. The superior performance of modal regression suggests that considering the conditional mode can lead to more accurate and precise predictions in the context of COVID-19 trend analysis.

5.2 Forecasting the Confirmed COVID-19 Cases by Modal Autoregression

Using the MAR method, we analyze the transformed COVID-19 cases $Y'_{(\cdot)}$ from Canada, Japan, Korea, and the U.S. for forecasting purposes. Before applying the MAR method, we perform the augmented Dickey-Fuller (ADF) test to examine the presence of a unit root in the series. If the unit-root hypothesis cannot be rejected, we take the first difference of the series and conduct the ADF test again. We repeat this procedure until we obtain evidence to reject the unit-root hypothesis. This iterative process allows us to identify the appropriate order of differencing needed for the time series data. By ensuring stationarity in the data, we can apply the MAR method effectively for forecasting COVID-19 cases.

Table 5 presents the results of the ADF test conducted on the original series and the series that has undergone three levels of differencing. The p-values obtained from the ADF test for the original series are all greater than 0.01, indicating that we cannot reject the null hypothesis of a unit root for these series. However, for the three-times differenced series, the p-values are all less than 0.01, providing evidence to reject the unit-root hypothesis. Based on these results, we proceed to specify the MAR model for the three-times differenced data and estimate the unknown parameters using the modal regression approach. The MAR order is determined by minimizing the BIC, as described in Section 3.2. In this case, we find that an MAR order of 6 is selected for all four countries.

<Insert Table 5 around here>

We assess the performance of the forecasts obtained from the MAR model estimation by comparing them with the forecasts obtained from the MEAR and LQAR models. To evaluate the forecasts on the training data, we compare the forecasts with the actual observations and compute the RMSE, MAE, and CQF. For evaluating the forecasts on the test data, we employ two approaches. First, we forecast the future values sequentially by using the recent forecasts as inputs (non-teacher-forcing method). Second, we forecast the future values by utilizing the recent realizations from the test data as inputs (teacher-forcing method). The teacher-forcing method is expected to produce more accurate forecasts compared to the non-teacher-forcing method since forecast errors tend to accumulate over the forecasting period. By employing these evaluation methods, we can assess the precision and accuracy of the MAR model forecasts and compare them with the MEAR and LQAR models.

We present the qualitative forecasting results obtained from the MAR model using the teacher-forcing method. The upper four panels of Figure 6 display these results. The MAR coefficients are estimated through modal regression with the bandwidth selected as SJ's bandwidth. It is evident that the MEAR, LQAR, and MAR models exhibit impressive forecasting performance in capturing the trend of the cumulative confirmed COVID-19 cases. Furthermore, the lower four panels of Figure 6 exhibit the forecasting results obtained through the non-teacher-forcing method. These results demonstrate a similar pattern to the forecasting results observed in the upper panels.

<Insert Figure 6 around here>

We provide a visual comparison of the daily forecasts for the cumulative confirmed COVID-19 cases in Figure 6. It is important to note that differencing the cumulative confirmed cases results in the forecast of daily confirmed cases. To visualize the daily forecast, we present Figure 7, which displays the daily forecast for the four countries. We summarize the results as follows:

(a) For both the teacher-forcing and non-teacher-forcing methods, we observe that the MAR method accurately captures the trends and autocorrelation patterns in the daily confirmed cases. Specifically, for the U.S., the series exhibits a declining trend with oscillation, while the series for Japan shows an initial decline followed by a rebound. These patterns are accurately captured by the MAR model, demonstrating its superior performance compared to the MEAR and LQAR models.

(b) For both the teacher-forcing and non-teacher-forcing methods, we observe that the MAR method outperforms the MAR and MEAR models in forecasting outliers. In Figure 7, we can see that the MAR forecasts show wider variations compared to the LQAR and MEAR forecasts. This indicates that the MAR forecasts are better able to capture the cyclical peaks and bottoms of the daily confirmed

cases. This trend is particularly evident for Canada and Japan.

(c) The forecast error on the test set tends to be larger in the non-teacher-forcing method compared to the teacher-forcing method. This is due to the fact that in the non-teacher-forcing method, the prediction errors accumulate as the last-period forecast is used as a covariate for the next-period forecast. This can lead to compounding errors and potentially larger forecast errors over time. On the other hand, in the teacher-forcing method, the use of actual realizations in the test data as inputs for forecasting helps mitigate the accumulation of errors, resulting in generally more accurate forecasts.

(d) Based on the forecast results obtained from the MAR, LQAR, and MEAR models, it can be concluded that governments can be better prepared when forecasting daily confirmed cases using the MAR model compared to the LQAR and MEAR models. The MAR model demonstrates better performance in capturing the trends, autocorrelation patterns, and outliers in the daily confirmed cases. This implies that relying on the MAR model for forecasting can provide governments with more accurate and reliable information to make informed decisions and take appropriate measures in response to the COVID-19 pandemic. □

<Insert Figure 7 around here>

The qualitative prediction outcomes for daily confirmed cases using the MAR model estimated by the modal regression with Scott's and Silverman's bandwidths are presented in Figures 8 and 9. Only the forecasts obtained by the teacher-forcing method are shown for brevity, and they exhibit similar performance to the forecasts obtained using SJ's bandwidth. However, it should be noted that there are significant differences in quantitative evaluations. Table 6 reports the RMSEs between the forecasts and the actual values obtained by the teacher-forcing method. It is observed that SJ's method outperforms the other two methods, which is consistent with the findings in Section 4.

<Insert Table 6 and Figures 8 and 9 around here>

The quantitative results of the three methods are reported in Tables 6 and 7. Table 6 displays the estimated parameters obtained using SJ's, Scott's, and Silverman's bandwidths for the MAR model, while Table 7 presents the performance measures of the MEAR, LQAR, and MAR models, including the RMSE, MAE, and CQF. We summarize the quantitative results as follows:

(a) Table 6 shows that SJ's bandwidth outperforms the other two methods (Scott's and Silverman's) in terms of RMSE for Canada, Japan, Korea, and the U.S. The estimated coefficients are generally similar across different bandwidths for Canada, Korea, and the U.S., while Japan exhibits notable differences among the different bandwidths.

(b) Table 7 indicates that for the training sets of the four countries, the CQF for the MAR model consistently has the smallest value. In terms of the test set, the MAR model performs relatively better than the MEAR and LQAR models in terms of the CQF.

(c) The MAR model consistently achieves the best CQF and sometimes even the best RMSE (Root Mean Squared Error) and MAE. This can be attributed to the robustness of the modal regression approach in handling unexpected noise and outliers present in the differenced data.

(d) The results obtained by the teacher-forcing method consistently outperform the forecast obtained by the non-teacher-forcing method. This validates our earlier discussion on the difference between these two methods, highlighting that the non-teacher-forcing method tends to accumulate forecast errors over the forecast horizon, leading to less accurate predictions compared to the teacher-forcing method.

□

<Insert Table 7 around here>

When comparing the performances of the different bandwidths for the four countries, it is evident that SJ's bandwidth consistently yields smaller RMSE values, indicating its superiority in forecasting the confirmed COVID-19 cases using the MAR method. Additionally, the smaller CQF values obtained by the MAR method compared to the MEAR and LQAR methods demonstrate that the MAER and LQAR methods are more sensitive to outliers and tend to accumulate forecasting errors gradually over time, affecting the overall forecast accuracy.

6 Conclusion

Since the outbreak of COVID-19, there has been a growing interest in analyzing its trend in the scientific literature. Over the years, our understanding of the disease and its development has improved as we have accumulated more data and gained more experience. In this context, the modal regression method has emerged as a valuable statistical tool for handling noisy and skewed data in predicting and analyzing the trend of the COVID-19 process. It allows us to account for the characteristics and fluctuations in the data, leading to more accurate predictions and insights into the dynamics of the disease.

In this study, the analysis of confirmed COVID-19 cases is carried out using the modal regression approach, which involves four main steps. First, an objective function is formulated to evaluate different forecasts for a series, considering the estimation of conditional mean, median, and mode. The forecasts are evaluated based on RMSE, MAE, and CQF metrics. The modal regression aims to optimize the CQF,

while conditional mean and median regressions optimize the RMSE and MAE, respectively. The CQF measures the probability of a random variable falling within a forecasted interval, making the conditional mode function suitable for optimizing the CQF. Second, a review of prediction models available in the literature is conducted, focusing on their application to modal regression. Two types of models, namely time-trend and unit-root models, are examined for their suitability in the modal regression framework. Third, simulations are performed to investigate the properties of the modal regression. The simulations involve cross-sectional and unit-root data, and the consistency of the modal regression is examined. It is discovered that the performance of the modal regression critically depends on the choice of bandwidth used to estimate the density function. Notably, the results demonstrate that SJ's bandwidth, along with Scott's and Silverman's bandwidths, provides robust estimation outcomes. Finally, the modal regression approach is applied to the analysis of confirmed COVID-19 cases in Canada, Japan, Korea, and the U.S. The empirical analysis aims to forecast and analyze the trends of COVID-19 cases using the modal regression framework, considering the characteristics and dynamics of the data for these countries.

Based on our empirical analysis, several key findings have emerged. First, the MR method consistently outperforms other methods in terms of CQF for the cumulative confirmed COVID-19 case data, regardless of whether time-trend or unit-root models are considered. For all four countries (Canada, Japan, Korea, and the U.S.), the CQF achieved through modal regression is consistently smaller than that of other methods, indicating better performance in terms of capturing the forecast uncertainty. Second, the forecasts obtained through modal regression demonstrate superior capability in capturing the cyclical peaks and bottoms of daily confirmed COVID-19 cases compared to mean and median regressions. This is attributed to the wider variation in the modal regression forecasts, which align more closely with the actual cyclical patterns. In contrast, the forecasts from mean and median regressions tend to underestimate and overestimate the cyclical peaks and bottoms, respectively. This finding has important implications from an economic standpoint, suggesting that the modal forecast can help governments avoid high risks when formulating health policies related to COVID-19 cases.

The research methodology employed in this study can be extended to analyze data from other countries or explore other infectious diseases. The methodology does not assume specific characteristics of the data from the four countries considered in this study and is established based on methodological considerations related to modal regression. Therefore, it can be applied to analyze various time series data.

However, it's important to note that the current study focuses on a single series and forecasting its future observations. It does not examine the interrelationship between two or more time-series variables. For instance, in the case of nonstationary data such as confirmed COVID-19 cases, it would be valuable to

investigate the cointegration and relationships with other variables. Exploring these interrelationships could be a potential direction for future research.

7 Appendix: Proof of $Q_{n,h}(\theta^{(k+1)}) \geq Q_{n,h}(\theta^{(k)})$

For each iteration of the MEM algorithm in Section 3.1, the optimized objective function outcome gradually increases. That is, for any positive integer k, $Q_{n,h}(\theta^{(k+1)}) \geq Q_{n,h}(\theta^{(k)})$. The proof is as follows: we note that

$$
\begin{aligned}
&\log Q_{n,h}\left(\theta^{(k+1)}\right) - \log Q_{n,h}\left(\theta^{(k)}\right) \\
&= \log \sum_{t=1}^{n} \phi_h\left(Y_t - m(X_t, \theta^{(k+1)})\right) - \log \sum_{t=1}^{n} \phi_h\left(Y_t - m(X_t, \theta^{(k)})\right) \\
&= \log \left[\sum_{t=1}^{n} \frac{\phi_h\left(Y_t - m(X_t, \theta^{(k+1)})\right)}{\sum_{j=1}^{n} \phi_h\left(Y_j - m(X_j, \theta^{(k)})\right)}\right] \\
&= \log \left[\sum_{t=1}^{n} \frac{\phi_h\left(Y_t - m(X_t, \theta^{(k)})\right)}{\sum_{t=1}^{n} \phi_h\left(Y_t - m(X_t, \theta^{(k)})\right)} \frac{\phi_h\left(Y_t - m(X_t, \theta^{(k+1)})\right)}{\phi_h(Y_t - m(X_t, \theta^{(k)}))}\right] \\
&= \log \left[\sum_{t=1}^{n} \pi(t \mid \theta^{(k)}) \frac{\phi_h\left(Y_t - m(X_t, \theta^{(k+1)})\right)}{\phi_h\left(Y_t - m(X_t, \theta^{(k)})\right)}\right]
\end{aligned}
$$

by noting that

$$
\pi(t \mid \theta^{(k)}) = \frac{\phi_h\left(Y_t - m(X_t, \theta^{(k)})\right)}{\sum_{t=1}^{n} \phi_h\left(Y_t - m(X_t, \theta^{(k)})\right)}.
$$

From this, we obtain

$$
\log Q_h\left(\theta^{(k+1)}\right) - \log Q_h\left(\theta^{(k)}\right) \geq \sum_{t=1}^{n} \pi(t \mid \theta^{(k)}) \log \left\{\frac{\phi_h\left(Y_t - m(X_t, \theta^{(k+1)})\right)}{\phi_h\left(Y_t - m(X_t, \theta^{(k)})\right)}\right\}
$$

by applying Jensen's inequality. If we further apply the definition of $\theta^{(k+1)}$ from the M-step,

$$
\sum_{t=1}^{n} \pi(t \mid \theta^{(k)}) \log \left\{\phi_h\left(Y_t - m(X_t, \theta^{(k+1)}\right))\right\} \geq \sum_{t=1}^{n} \pi(t \mid \theta^{(k)}) \log \left\{\phi_h\left(Y_t - m(X_t, \theta^{(k)}\right))\right\},
$$

implying that

$$
\log \left\{Q_h\left(\theta^{(k+1)}\right)\right\} - \log \left\{Q_h\left(\theta^{(k)}\right)\right\} \geq 0.
$$

This completes the proof. □

References

AJIDE, K. B., R. L. IBRAHIM, AND O. Y. ALIMI (2020): "Estimating the Impacts of Lockdown on COVID-19 Cases in Nigeria," *Transportation Research Interdisciplinary Perspectives*, 7, 100217.

ALMESHAL, A. M., A. I. ALMAZROUEE, M. R. ALENIZI, AND S. N. ALHAJERI (2020): "Forecasting the Spread of COVID-19 in Kuwait using Compartmental and Logistic Regression Models," *Applied Sciences*, 10, 3402.

ALMOND, D., X. DU, AND S. ZHANG (2020): *Did COVID-19 Improve Air Quality near Hubei?*, National Bureau of Economic Research Cambridge, Massachusetts.

ANDRÉE, B. P. J. (2020): "Incidence of COVID-19 and Connections with Air Pollution Exposure: Evidence from the Netherlands," *MedRxiv*, 2020–04.

AZIMLI, A. (2020): "The Impact of COVID-19 on the Degree of Dependence and Structure of Risk-Return Relationship: A Quantile Regression Approach," *Finance Research Letters*, 36, 101648.

BÉLAND, L.-P., A. BRODEUR, D. MIKOLA, AND T. WRIGHT (2022): "The Short-Term Economic Consequences of COVID-19: Occupation Tasks and Mental Health in Canada," *Canadian Journal of Economics*, 55, 214–247.

BÉLAND, L.-P., A. BRODEUR, AND T. WRIGHT (2023): "The Short-Term Economic Consequences of COVID-19: Exposure to Disease, Remote Work and Government Response," *Plos One*, 18, e0270341.

BOCCALETTI, S., W. DITTO, G. MINDLIN, AND A. ATANGANA (2020): "Modeling and Forecasting of Epidemic Spreading: The Case of COVID-19 and Beyond," *Chaos, Solitons, and Fractals*, 135, 109794.

BRODEUR, A., N. COOK, AND T. WRIGHT (2021a): "On the Effects of COVID-19 Safer-at-Home Policies on Social Distancing, Car Crashes and Pollution," *Journal of Environmental Economics and Management*, 106, 102427.

BRODEUR, A., D. GRAY, A. ISLAM, AND S. BHUIYAN (2021b): "A Literature Review of the Economics of COVID-19," *Journal of Economic Surveys*, 35, 1007–1044.

BUHAI, S. (2005): "Quantile Regression: Overview and Selected Applications," *Ad Astra*, 4, 1–17.

CAR, Z., S. BARESSI ŠEGOTA, N. ANĐELIĆ, I. LORENCIN, AND V. MRZLJAK (2020): "Modeling the Spread of COVID-19 Infection using a Multilayer Perceptron," *Computational and Mathematical Methods in Medicine*, 2020.

CHAKRABORTY, T. AND I. GHOSH (2020): "Real-Time Forecasts and Risk Assessment of Novel Coronavirus (COVID-19) Cases: A Data-Driven Analysis," *Chaos, Solitons & Fractals*, 135, 109850.

CHAN, S., J. CHU, Y. ZHANG, AND S. NADARAJAH (2021): "Count Regression Models for COVID-19," *Physica A: Statistical Mechanics and its Applications*, 563, 125460.

CHEN, Y.-C. (2018): "Modal Regression using Kernel Density Estimation: A Review," *Wiley Interdisciplinary Reviews: Computational Statistics*, 10, e1431.

CHEN, Y.-C., C. R. GENOVESE, R. J. TIBSHIRANI, AND L. WASSERMAN (2016): "Nonparametric Modal Regression," *Annals of Statistics*, 44, 489–514.

DEMPSTER, A. P., N. M. LAIRD, AND D. B. RUBIN (1977): "Maximum Likelihood from Incomplete Data via the EM Algorithm," *Journal of the Royal Statistical Society: Series B (Methodological)*, 39, 1–22.

GNING, L., C. NDOUR, AND J. TCHUENCHE (2022): "Modeling COVID-19 Daily Cases in Senegal using a Generalized Waring Regression Model," *Physica A: Statistical Mechanics and its Applications*, 597, 127245.

GUMAEI, A., M. AL-RAKHAMI, M. M. AL RAHHAL, F. ALBOGAMY, E. AL MAGHAYREH, AND H. ALSALMAN (2021): "Prediction of COVID-19 Confirmed Cases using Gradient Boosting Regression Method," *Computers, Materials & Continua*, 66, 315–329.

GUPTA, S., L. MONTENOVO, T. NGUYEN, F. LOZANO-ROJAS, I. SCHMUTTE, K. SIMON, B. A. WEINBERG, AND C. WING (2023): "Effects of Social Distancing Policy on Labor Market Outcomes," *Contemporary Economic Policy*, 41, 166–193.

HAMERMESH, D. S. (2020): "Life Satisfaction, Loneliness and Togetherness, with an Application to COVID-19 Lock-Downs," *Review of Economics of the Household*, 18, 983–1000.

HE, G., Y. PAN, AND T. TANAKA (2020): "COVID-19, City Lockdowns, and Air Pollution: Evidence from China," *MedRxiv*.

KHARDANI, S. AND A. F. YAO (2017): "Non Linear Parametric Mode Regression," *Communications in Statistics-Theory and Methods*, 46, 3006–3024.

KRIEF, J. M. (2017): "Semi-Linear Mode Regression," *The Econometrics Journal*, 20, 149–167.

LI, J., S. RAY, AND B. G. LINDSAY (2007): "A Nonparametric Statistical Approach to Clustering via Mode Identification," *Journal of Machine Learning Research*, 8, 1687–1723.

LU, H., P. NIE, AND L. QIAN (2021): "Do Quarantine Experiences and Attitudes towards COVID-19 Affect the Distribution of Mental Health in China? A Quantile Regression Analysis," *Applied Research in Quality of Life*, 16, 1925–1942.

MOLLALO, A., K. M. RIVERA, AND B. VAHEDI (2020): "Artificial Neural Network Modeling of Novel Coronavirus (COVID-19) Incidence Rates across the Continental United States," *International Journal of Environmental Research and Public Health*, 17, 4204.

MUSULIN, J., S. BARESSI ŠEGOTA, D. ŠTIFANIĆ, I. LORENCIN, N. ANĐELIĆ, T. ŠUŠTERŠIČ, A. BLAGOJEVIĆ, N. FILIPOVIĆ, T. ĆABOV, AND E. MARKOVA-CAR (2021): "Application of Artificial Intelligence-Based Regression Methods in the Problem of COVID-19 Spread Prediction: A Systematic Review," *International Journal of Environmental Research and Public Health*, 18, 4287.

OLMSTEAD, T. A. M. D. J. AND R. M. TERTILT (2020): "The Impact of COVID-19 on Gender Equality," Tech. Rep. 26947, National Bureau of Economic Research.

PORTER, S. R. (2015): "Quantile Regression: Analyzing Changes in Distributions instead of Means," *Higher Education: Handbook of Theory and Research*, 335–381.

ROJAS, F. L., X. JIANG, L. MONTENOVO, K. I. SIMON, B. A. WEINBERG, AND C. WING (2020): "Is the Cure Worse than the Problem Itself? Immediate Labor Market Effects of COVID-19 Case Rates and School Closures in the US," Tech. Rep. 27127, National Bureau of Economic Research.

SALGOTRA, R., M. GANDOMI, AND A. H. GANDOMI (2020a): "Evolutionary Modelling of the COVID-19 Pandemic in Fifteen Most Affected Countries," *Chaos, Solitons & Fractals*, 140, 110118.

——— (2020b): "Time series Analysis and Forecast of the COVID-19 Pandemic in India using Genetic Programming," *Chaos, Solitons & Fractals*, 138, 109945.

SASAKI, H., T. SAKAI, AND T. KANAMORI (2020): "Robust Modal Regression with Direct Gradient Approximation of Modal Regression Risk," in *Proceedings of the Thirty-Sixth Conference on Uncertainty in Artificial Intelligence, UAI 2020, virtual online, August 3-6, 2020*, ed. by R. P. Adams and V. Gogate, AUAI Press, vol. 124 of *Proceedings of Machine Learning Research*, 380–389.

SCOTT, D. W. (1979): "On Optimal and Data-Based Histograms," *Biometrika*, 66, 605–610.

SHEATHER, S. J. AND M. C. JONES (1991): "A Reliable Data-Based Bandwidth Selection Method for Kernel Density Estimation," *Journal of the Royal Statistical Society: Series B (Methodological)*, 53, 683–690.

SILVERMAN, B. W. (1986): *Density Eestimation for Statistics and Data Analysis*, vol. 26, CRC press.

TUBADJI, A., F. BOY, AND D. WEBBER (2020): "Narrative Economics, Public Policy and Mental Health," *Center for Economic Policy Research*, 20, 109–131.

ULLAH, A., T. WANG, AND W. YAO (2021): "Modal Regression for Fixed Effects Panel Data," *Empirical Economics*, 60, 261–308.

——— (2022): "Nonlinear Modal Regression for Dependent Data with Application for Predicting COVID-19." *Journal of the Royal Statistical Society: Series A (Statistics in Society)*, 185, 1424–1453.

VESPIGNANI, A., H. TIAN, C. DYE, J. O. LLOYD-SMITH, R. M. EGGO, M. SHRESTHA, S. V. SCARPINO, B. GUTIERREZ, M. U. KRAEMER, J. WU, ET AL. (2020): "Modelling COVID-19," *Nature Reviews Physics*, 2, 279–281.

XIANG, S. AND W. YAO (2022): "Nonparametric Statistical Learning Based on Modal Regression," *Journal of Computational and Applied Mathematics*, 409, 114130.

YAO, W. AND L. LI (2014): "A New Regression Model: Modal Linear Regression," *Scandinavian Journal of Statistics*, 41, 656–671.

YOUSEFPOUR, A., H. JAHANSHAHI, AND S. BEKIROS (2020): "Optimal Policies for Control of the Novel Coronavirus Disease (COVID-19) Outbreak," *Chaos, Solitons & Fractals*, 136, 109883.

YU, P., Z. ZHU, J. SHI, AND X. AI (2020): "Robust Estimation for Partial Functional Linear Regression Model Based on Modal Regression," *Journal of Systems Science and Complexity*, 33, 527–544.

ZHOU, H. AND X. HUANG (2016): "Nonparametric Modal Regression in the Presence of Measurement Error," *Electronic Journal of Statistics*, 10, 3579–3620.

——— (2019): "Bandwidth Selection for Nonparametric Modal Regression," *Communications in Statistics-Simulation and Computation*, 48, 968–984.

ZIVKOVIC, M., N. BACANIN, A. DJORDJEVIC, M. ANTONIJEVIC, I. STRUMBERGER, T. A. RASHID, ET AL. (2021): "Hybrid Genetic Algorithm and Machine Learning Method for COVID-19 Cases Prediction," in *Proceedings of International Conference on Sustainable Expert Systems*, Springer, 169–184.

	Hospital Beds per 1,000 People (as of 2020)	Health Expenditure Growth between 2019 and 2020 (as % of GDP)	Cumulative Vaccinations per 100 People (as of Dec. 2022)	Fatality Rate (as of Dec,2022)
Canada	2.79	1.99% pt.	247.84	1.1% (48,349)
Japan	12.63	0.15% pt.	285.44	0.2% (50,827)
Korea	12.65	0.22% pt.	250.19	0.1% (30,975)
U.S.	2.80	2.14% pt.	197.37	1.1% (1,083,362)

Table 1: MEDICAL STATISTICS ON COVID-19 FOR THE FOUR COUNTRIES.The data of Hospital Beds is sourced from Trading Economics (https://tradingeconomics.com/country-list/hospital-beds). The data of Health Expenditure is sourced from The World Bank (https://data.worldbank.org/indicator). The data of Cumulative Vaccinations and fatality rate are sourced from Our World in Data (https://ourworldindata.org/covid-vaccinations).

	Method	Parameter $\backslash$ n	100	200	300	500	1,000
DGP1	MER	α_{1*}	0.3381	0.1625	0.1074	0.0661	0.0311
		β_{1*}	1.0970	0.5511	0.3604	0.2270	0.1035
	LQR	α_{2*}	0.3677	0.1735	0.1259	0.0717	0.0346
		β_{2*}	1.2485	0.6062	0.4221	0.2450	0.1170
	MR & SJ	α_{3*}	0.4563	0.3721	0.3721	0.1467	0.0923
		β_{3*}	0.9167	0.8285	0.7511	0.5574	0.2566
	MR & Scott	α_{3*}	0.4662	0.3792	0.3784	0.1462	0.0914
		β_{3*}	0.9257	0.8849	0.7663	0.5667	0.2673
	MR & Silverman	α_{3*}	0.5047	0.4511	0.4200	0.1531	0.1008
		β_{3*}	1.1022	1.0236	0.8921	0.6430	0.2592
DGP2	MER	α_{4*}	0.2541	0.1167	0.0791	0.0467	0.0231
		β_{4*}	0.7455	0.3613	0.2357	0.1331	0.0725
	LQR	α_{5*}	0.2818	0.1340	0.0918	0.0536	0.0271
		β_{5*}	0.8637	0.3867	0.2764	0.1669	0.0805
	MR & SJ	α_{6*}	1.9091	1.7029	1.3450	1.3166	1.2781
		β_{6*}	2.8691	2.5467	2.1244	2.0269	1.8912
	MR & Scott	α_{6*}	1.9723	1.7681	1.4101	1.4293	1.2901
		β_{6*}	2.7920	2.5719	2.2965	2.2910	1.9801
	MR & Silverman	α_{6*}	2.0121	1.7921	1.3771	1.3491	1.3291
		β_{6*}	2.8812	2.7021	2.3103	2.1310	1.9004

Table 2: THE MSES USING THE CROSS-SECTIONAL DATA SIMULATIONS. DGP1 is generated by simulating IID samples $\{(X_t, Y_t), i = 1, \ldots, n\}$ such thatt $Y_t = \alpha_* + \beta_* X_t + U_t$, where $\alpha_* = 0$, $\beta_* = 2$, and $U_t \sim 0.5N(-2, 3^2) + 0.5N(2, 1^2)$, from which $\mathbb{E}(Y_t \mid X_i) = 2X_t$, median $(Y_t \mid X_i) = 2X_t + 1$, and mode $(Y_t \mid X_i) = 2X_t + 2$. DGP2 is generated by simulating IID samples such that $Y_t = \alpha_* + \beta_* X_t + U_t$, where $\alpha_* = 0$, $\beta_* = 1$, and $U_t \sim \mathcal{X}_3^2 - 3$, from which $\mathbb{E}(Y_t \mid X_i) = X_t$, median $(Y_t \mid X_i) = X_t - 0.63$, and mode $(Y_t \mid X_i) = X_t - 2$. The simulation results are obtained by conducting 1,000 replications.

Method	Parameter $\setminus n$	100	200	300	500	1,000
MEAR	α_{7*}	0.1472	0.0305	0.0284	0.0337	0.0382
	β_{7*}	0.0009	0.0000	0.0001	0.0000	0.0000
LQAR	α_{8*}	0.4024	0.2732	0.1771	0.1185	0.1017
	β_{8*}	2.4436	1.3439	1.4007	1.2859	1.0010
MAR & SJ	α_{9*}	0.2624	0.1978	0.1929	0.1561	0.0309
	β_{9*}	0.0009	0.0006	0.0007	0.0007	0.0000
MAR & Scott	α_{9*}	0.2821	0.1799	0.2581	0.2178	0.0312
	β_{9*}	0.0009	0.0009	0.0011	0.0010	0.0000
MAR & Silverman	α_{9*}	0.3819	0.2953	0.2734	0.2853	0.1339
	β_{9*}	0.0014	0.0009	0.0009	0.0007	0.0004

Table 3: THE MSES USING THE TIME-SERIES DATA SIMULATIONS. This table compares the performances from different estimations: MEAR, LQAR, and MAR methods based upon the SJ's Scott's, and Silverman's bandwidths. The simulated data set $\{Y_t : t = 1, \ldots, n\}$ is obtained from the following DGP: $Y_t = \alpha_* + \beta_* Y_{t-1} + U_t$, where $\alpha_* = 0$, $\beta_* = 1$ and $U_t \sim 0.3N(-2, 3^2) + 0.2N(2, 2^2) + 0.5N(1, 1^2)$. From this, $\mathbb{E}(Y_t \mid Y_{t-1}) = 0.3 + Y_{t-1}$, median $(Y_t \mid Y_{t-1}) = 0.75 + Y_{t-1}$, and mode $(Y_t \mid Y_{t-1}) = 1 + Y_{t-1}$.

Country	Method	Training Set			Test Set		
		RMSE	MAE	CQF	RMSE	MAE	CQF
Canada	MER	0.0148	0.0118	0.0103	0.0318	0.0304	0.0298
	LQR	0.0152	0.0111	0.0085	0.0354	0.0342	0.0332
	MR	0.0148	0.0117	0.0102	0.0319	0.0306	0.0299
	BMR	0.0063	0.0051	**0.0038**	0.0709	0.0531	0.0466
	LPMR	0.0063	0.0052	0.0043	0.0171	0.0146	**0.0124**
Japan	MER	0.0303	0.0267	0.0275	0.0756	0.0749	0.0755
	LQR	0.0326	0.0250	0.0168	0.0838	0.0832	0.0838
	MR	0.0303	0.0265	0.0165	0.0758	0.0750	0.0757
	BMR	0.0033	0.0027	0.0024	0.0083	0.0069	**0.0045**
	LPMR	0.0031	0.0025	**0.0023**	0.0125	0.0115	0.0103
Korea	MER	0.0621	0.0551	0.0583	0.0961	0.0960	0.0958
	LQR	0.0644	0.0543	0.0537	0.0643	0.0639	0.0619
	MR	0.0706	0.0555	0.0496	0.0550	0.0541	0.0517
	BMR	0.0043	0.0028	**0.0014**	0.0823	0.0690	0.0532
	LPMR	0.0036	0.0026	0.0018	0.0870	0.0605	**0.0399**
U.S.	MER	0.0646	0.0531	0.0490	0.1238	0.1221	0.1295
	LQR	0.0722	0.0486	0.0332	0.0912	0.0898	0.0947
	MR	0.0749	0.0489	0.0336	0.0779	0.0765	0.0805
	BMR	0.0072	0.0049	0.0035	0.0283	0.0221	**0.0147**
	LPMR	0.0070	0.0047	**0.0030**	0.0251	0.0204	**0.0147**

Table 4: THE QUANTITATIVE RESULTS OF DIFFERENT ESTIMATION METHODS. This table evaluates the efficacy of different regression methods for forecasting the cumulative confirmed COVID-19 cases from February 8, 2022 to April 8, 2022. The results are measured by RMSE, MAE and CQF.

Country	Before			After		
	Dickey-Fuller	p-value	Reject	Dickey-Fuller	p-value	Reject
Canada	-3.0538	0.1516	No	-6.4527	< 0.01	Yes
Japan	-0.9009	0.9447	No	-5.4706	< 0.01	Yes
Korea	-1.9200	0.6064	No	-5.5924	< 0.01	Yes
U.S.	-4.0388	0.0151	No	-5.8077	< 0.01	Yes

Table 5: THE RESULTS OF THE ADF TEST BEFORE AND AFTER DIFFERENCING THE ACCUMULATED CONFIRMED COVID-19 CASES. The considered data set ranges from February 8, 2022 to April 8, 2022, and the ADF test significance level is set to 0.01. To ensure the stationarity of the time series, we set the difference order be 3.

Method			Canada	Japan	Korea	U.S.
SJ	RMSE	Training Set	**0.1764**	**0.1350**	**0.1085**	0.0355
		Test Set	**0.2857**	**0.0699**	**0.0701**	**0.0307**
	Coef	α_*	-0.0236	-0.0044	0.0000	0.0029
		β_{1*}	-0.5224	-0.9021	-0.8679	-0.5925
		β_{2*}	-0.3358	-0.8722	-1.0773	-0.6856
		β_{3*}	-0.6016	-0.8328	-1.3416	-0.7422
		β_{4*}	-1.1054	-0.7654	-1.3734	-0.8425
		β_{5*}	-1.3693	-0.8430	-1.4871	-0.9307
		β_{6*}	-1.3588	-0.7832	-1.2355	-0.9529
Scott	RMSE	Training Set	0.1779	0.1450	0.1279	0.0355
		Test Set	0.2889	0.1044	0.0929	0.0308
	Coef	α_*	-0.0234	0.0526	0.0035	0.0029
		β_{1*}	-0.5289	-0.4999	-1.1798	-0.5953
		β_{2*}	-0.3329	-0.9829	-1.0942	-0.6893
		β_{3*}	-0.6020	-1.0668	-1.2720	-0.7473
		β_{4*}	-1.1118	-1.1104	-1.1384	-0.8464
		β_{5*}	-1.3744	-1.0587	-1.3406	-0.9316
		β_{6*}	-1.3638	-0.9479	-1.0740	-0.9527
Silverman	RMSE	Training Set	0.1799	0.1506	0.1093	**0.0354**
		Test Set	0.2907	0.1069	0.0806	0.0308
	Coef	α_*	-0.0235	0.0509	-0.0088	0.0025
		β_{1*}	-0.5364	-0.4543	-0.5419	-0.5885
		β_{2*}	-0.3288	-0.9954	-0.6828	-0.6800
		β_{3*}	-0.5997	-1.1023	-0.9043	-0.7340
		β_{4*}	-1.1199	-1.1617	-0.7628	-0.8361
		β_{5*}	-1.3785	-1.0871	-1.1533	-0.9277
		β_{6*}	-1.3723	-0.9580	-0.9320	-0.9529

Table 6: THE QUANTITATIVE RESULTS OF DIFFERENT BANDWIDTH SELECTION METHODS FOR COVID-19. The RMSE is computed by comparing the forecasts with the realized confirmed cases. Here, α_* denotes the intercept, and the lag coefficients are denoted as β_{1*}, β_{2*}, β_{3*}, β_{4*}, β_{5*}, and β_{6*}.

Country	Method	Training Set			Test Set (Teacher Forcing)			Test Set (Non-teacher Forcing)		
		RMSE	MAE	CQF	RMSE	MAE	CQF	RMSE	MAE	CQF
Canada	MEAR	0.1443	0.1145	0.1043	0.2206	0.1968	**0.1784**	0.2745	0.2243	0.1991
	LQAR	0.1487	0.1120	0.0930	0.2494	0.2124	0.1898	0.2373	0.2004	0.1893
	MAR	0.1764	0.1256	**0.0664**	0.2857	0.2338	0.1855	0.1981	0.1794	**0.1855**
Japan	MEAR	0.1151	0.0906	0.0656	0.0625	0.0535	0.0492	0.2359	0.2185	0.2776
	LQAR	0.1201	0.0834	0.0510	0.0609	0.0487	0.0416	0.3254	0.3039	0.2822
	MAR	0.1350	0.0883	**0.0404**	0.0699	0.0538	**0.0396**	0.3796	0.3574	**0.2541**
Korea	MEAR	0.1027	0.0647	0.0348	0.0757	0.0593	0.0400	0.0675	0.0532	0.0748
	LQAR	0.1059	0.0624	0.0349	0.0967	0.0791	0.0806	0.0835	0.0707	0.0819
	MAR	0.1085	0.0654	**0.0217**	0.0701	0.0506	**0.0360**	0.0781	0.0653	**0.0654**
U.S.	MEAR	0.0342	0.0256	0.0197	0.0303	0.0211	0.0136	0.0302	0.0225	**0.0135**
	LQAR	0.0348	0.0247	0.0189	0.0315	0.0219	0.0168	0.0463	0.0295	0.0180
	MAR	0.0355	0.0251	**0.0157**	0.0307	0.0198	**0.0133**	0.0291	0.0212	0.0141

Table 7: THE QUANTITATIVE RESULTS OF THE FORECAST METHODS. This table compares the performances of the MEAR, LQR, and MAR methods applied to the cumulative confirmed COVID-19 cases. That data range from February 8, 2022 to April 8, 2022. For the test data set, the teacher-forcing and non-teacher-forcing methods are separately applied.

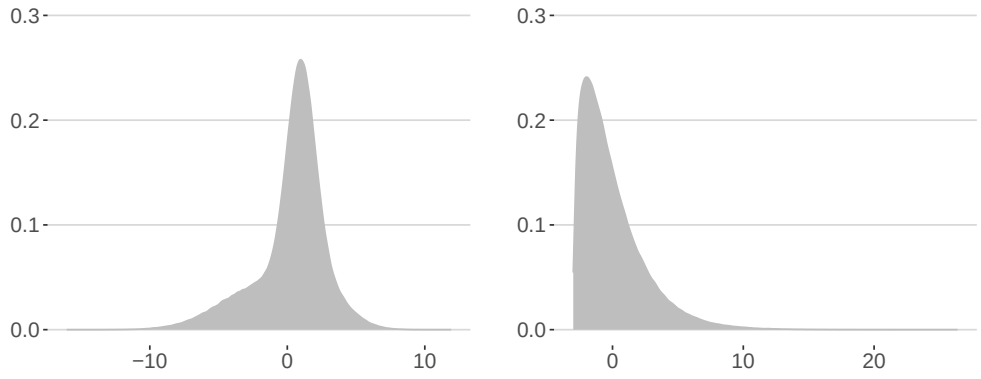

(a) DGP1 (b) DGP2

Figure 1: THE PROBABILITY DENSITY FUNCTION OF THE ERROR DISTRIBUTION IN THE DGPS. The skewed error of DGP1 is generated from $U_t \sim 0.5N(-2, 3^2) + 0.5N(2, 1^2)$. The skewed error of DGP2 is generated from $U_t \sim \mathcal{X}_3^2 - 3$.

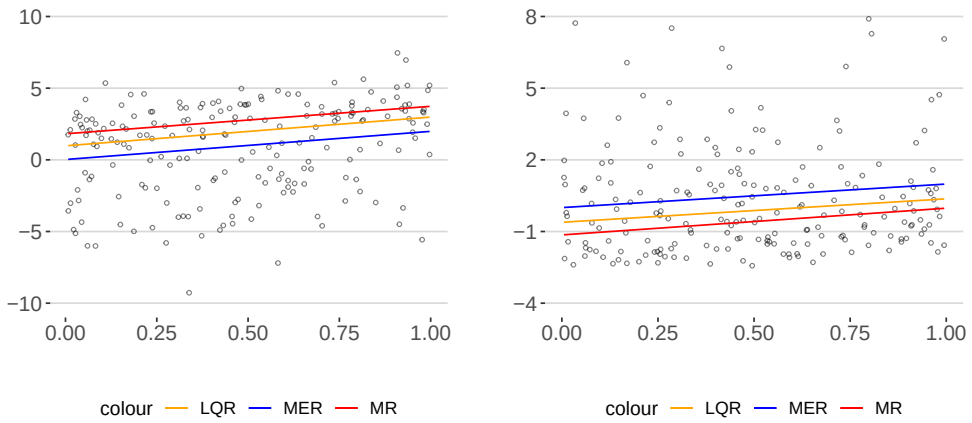

(a) DGP1 (b) DGP2

Figure 2: THE SCATTER PLOT AND REGRESSION LINES. 200 data points are generated from DGP1: $Y_t = \alpha_* + \beta_* X_t + U_t$, where $\alpha_* = 0$, $\beta_* = 2$ and $U_t \sim 0.5N(-2, 3^2) + 0.5N(2, 1^2)$. The red line represents conditional mode function; the orange line represents the conditional median function; and the blue line represents the conditional mean function. Other 200 data points are generated from DGP2: $Y_t = \alpha_* + \beta_* X_t + U_t$, where $\alpha_* = 0$, $\beta_* = 1$ and $U_t \sim \mathcal{X}_3^2 - 3$. The red line represents modal regression, the orange line represents median regression and the blue line represents mean regression.

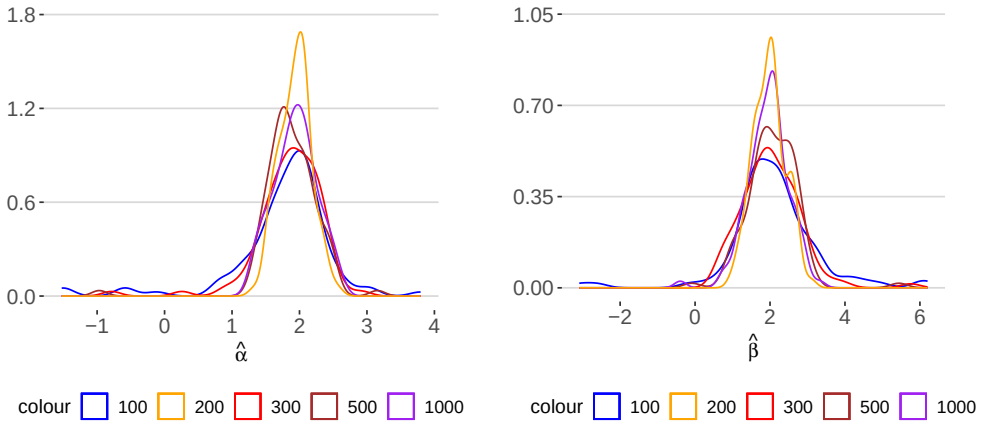

(a) $\widehat{\alpha}_n$ of DGP1

(b) $\widehat{\beta}_n$ of DGP1

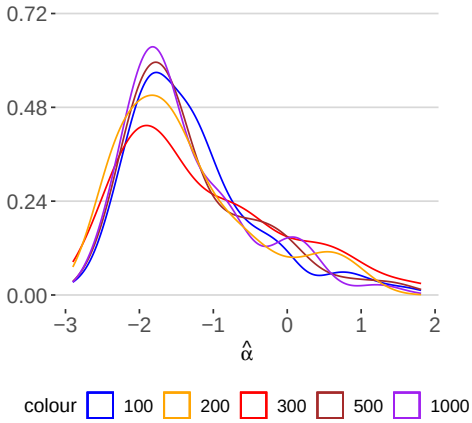

(c) $\widehat{\alpha}_n$ of DGP2

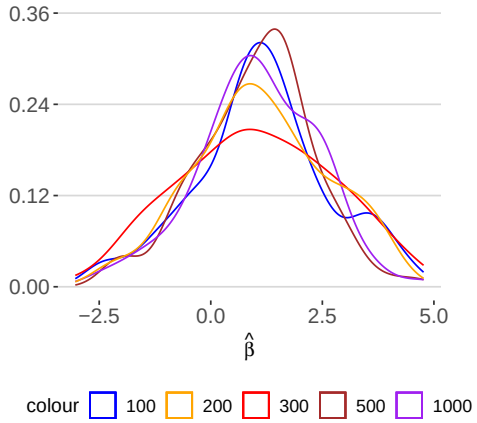

(d) $\widehat{\beta}_n$ of DGP2

Figure 3: EMPIRICAL DENSITY OF THE MODAL REGRESSION COEFFICIENTS FROM THE CROSS-SECTIONAL DATA. The four figures display the probability density of the estimated coefficients $\widehat{\alpha}_n$ and $\widehat{\beta}_n$ for the cross-sectional data separately.

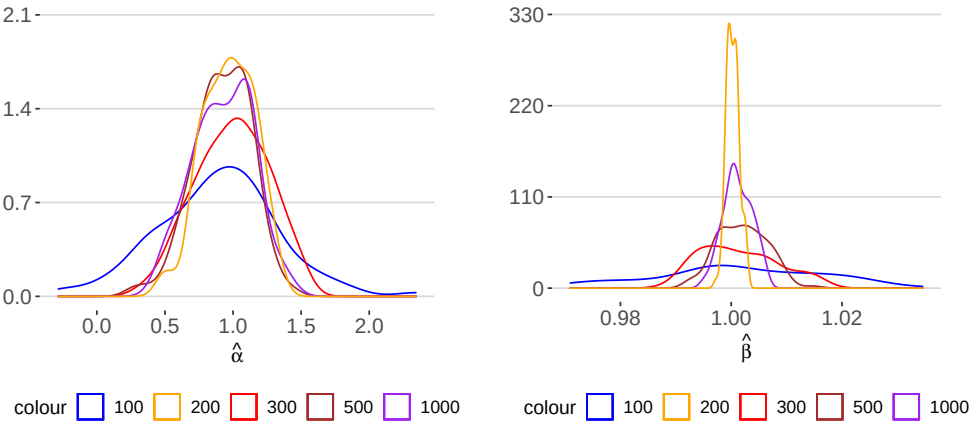

(a) DGP1 (b) DGP2

Figure 4: EMPIRICAL DENSITY OF THE MODAL REGRESSION COEFFICIENTS FROM THE TIME-SERIES DATA. The two figures separately show the probability density of the estimated coefficients $\widehat{\alpha}_n$ and $\widehat{\beta}_n$ of the time series data.

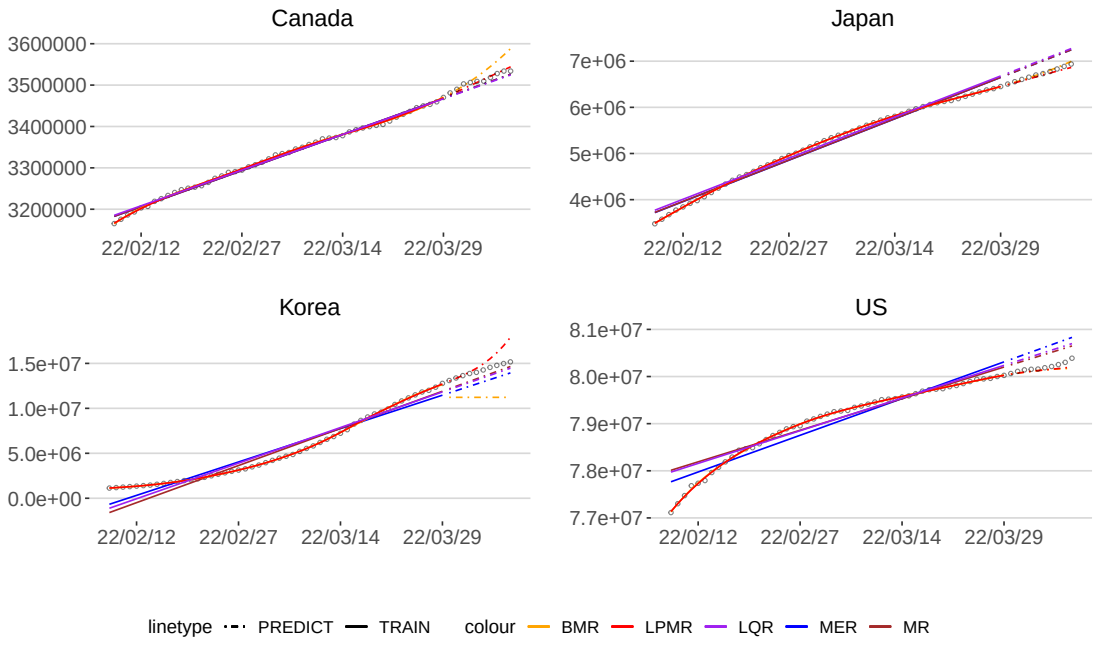

Figure 5: THE SCATTER PLOT OF ALL DATA POINTS AND THE REGRESSION LINES FROM THE DIFFERENT REGRESSION METHODS. This figure shows different forecasts from the five regression methods: MER, LQR, MR, BMR, and LPMR. The vertical axis denotes the number of the cumulative confirmed COVID-19 cases.

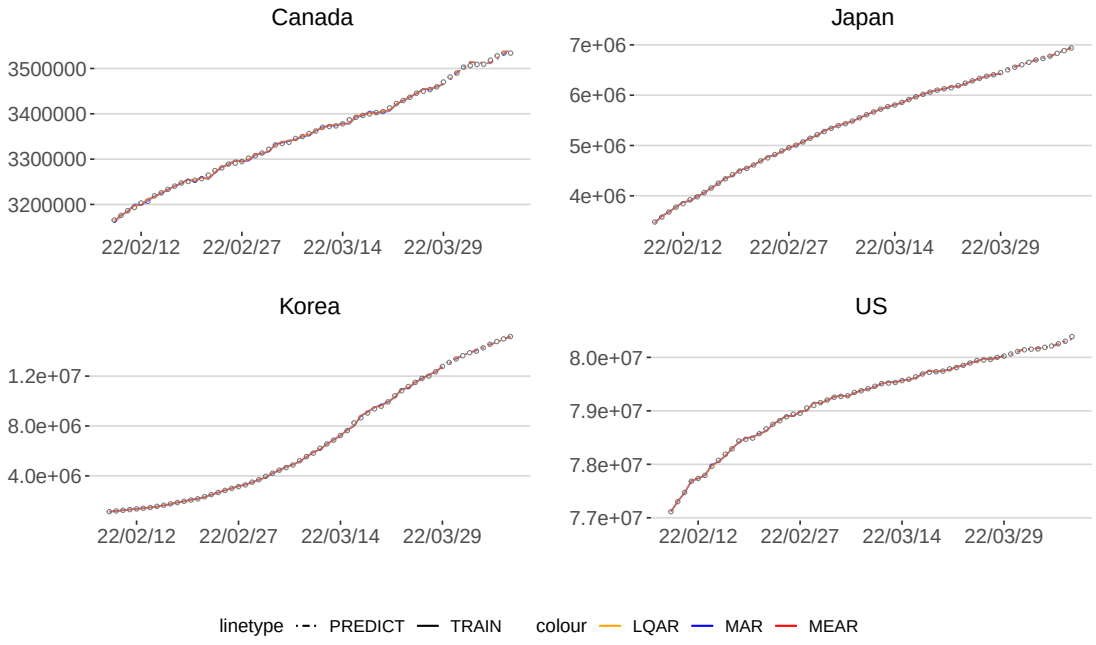

(a) Teacher-Forcing Method

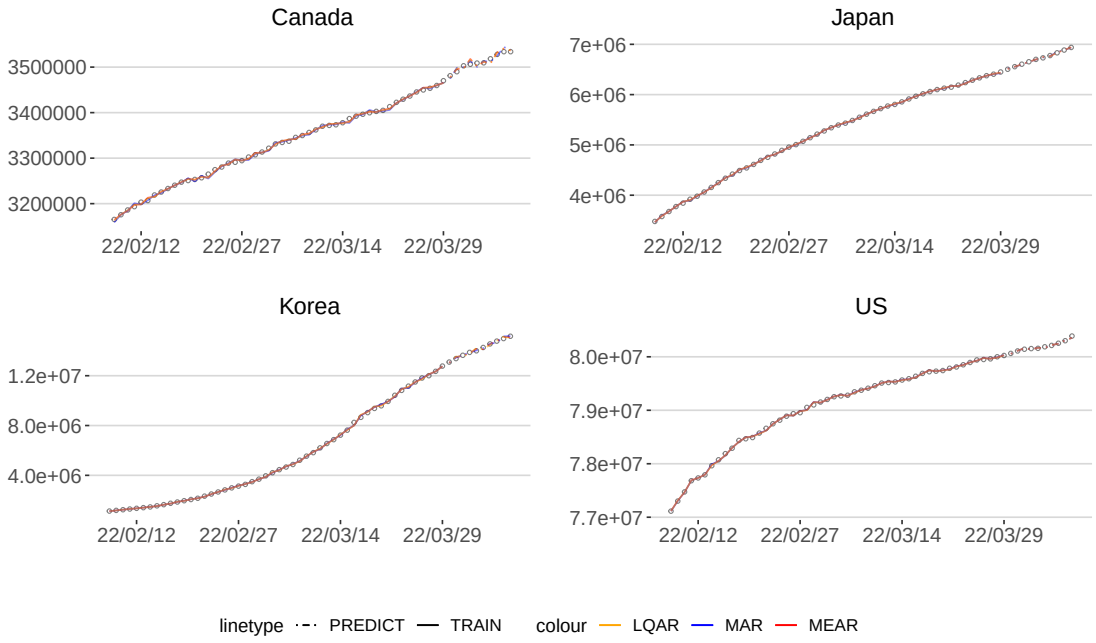

(b) Non-Teacher-Forcing Method

Figure 6: THE QUALITATIVE FORECASTING RESULTS OF THE MEAR, LQAR AND MAR METHODS ON THE ACCUMULATED CONFIRMED CASES. The red, orange, and blue line represent the forecasting made by the MEAR, LQAR, and MAR methods, respectively using the teacher-forcing and non-teacher-forcing methods.

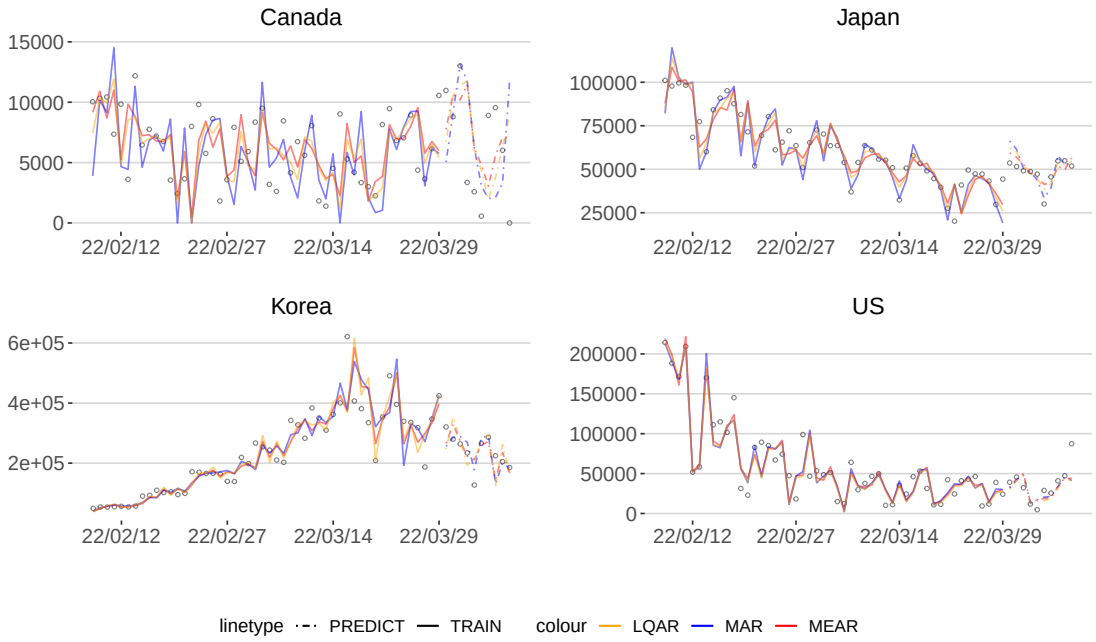

(a) Teacher-Forcing Method

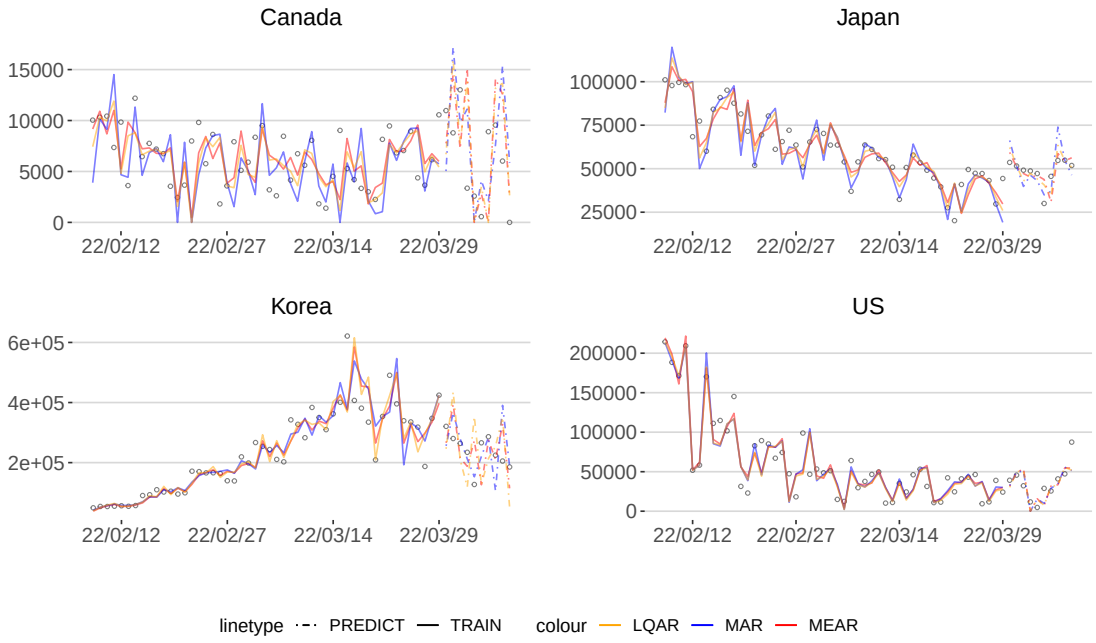

(b) Non-Teacher-Forcing Method

Figure 7: THE QUALITATIVE FORECASTING RESULTS OF THE MEAR, LQAR AND MAR METHODS ON THE DAILY CONFIRMED CASES. The red, orange, and blue line represent the forecasting made by the MEAR, LQAR, and MAR methods, respectively using the teacher-forcing and non-teacher-forcing methods with SJ's bandwidth.

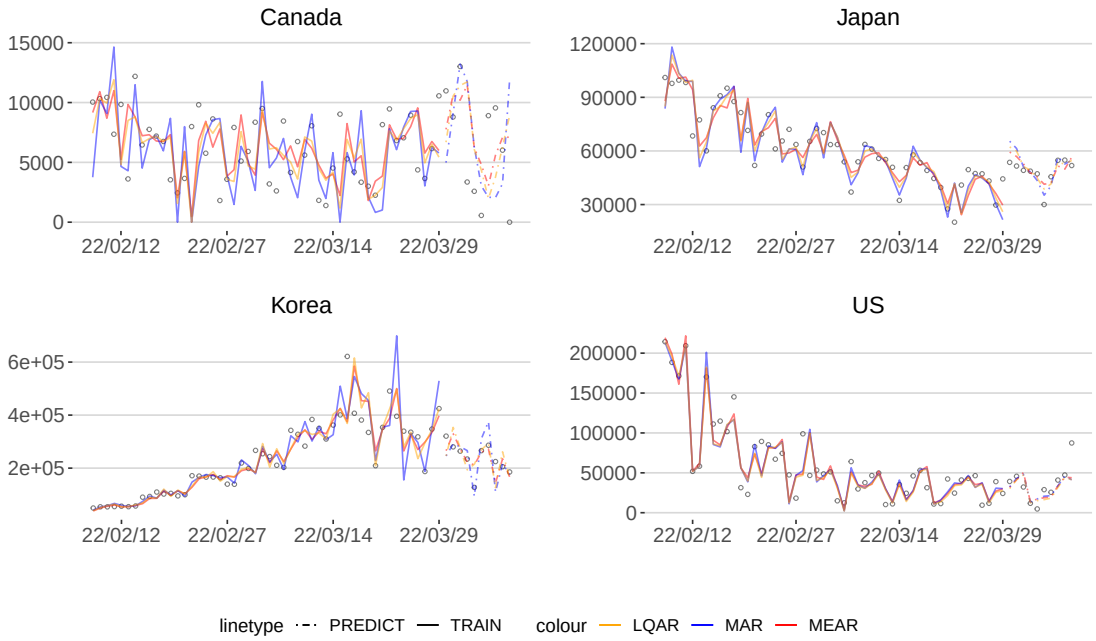

Figure 8: THE QUALITATIVE FORECASTING RESULTS OF THE MEAR, LQAR AND MAR METHODS ON THE DAILY CONFIRMED CASES. The red, orange, and blue line represent the forecasting made by the MEAR, LQAR, and MAR methods, respectively using the teacher-forcing method and Scott's bandwidth.

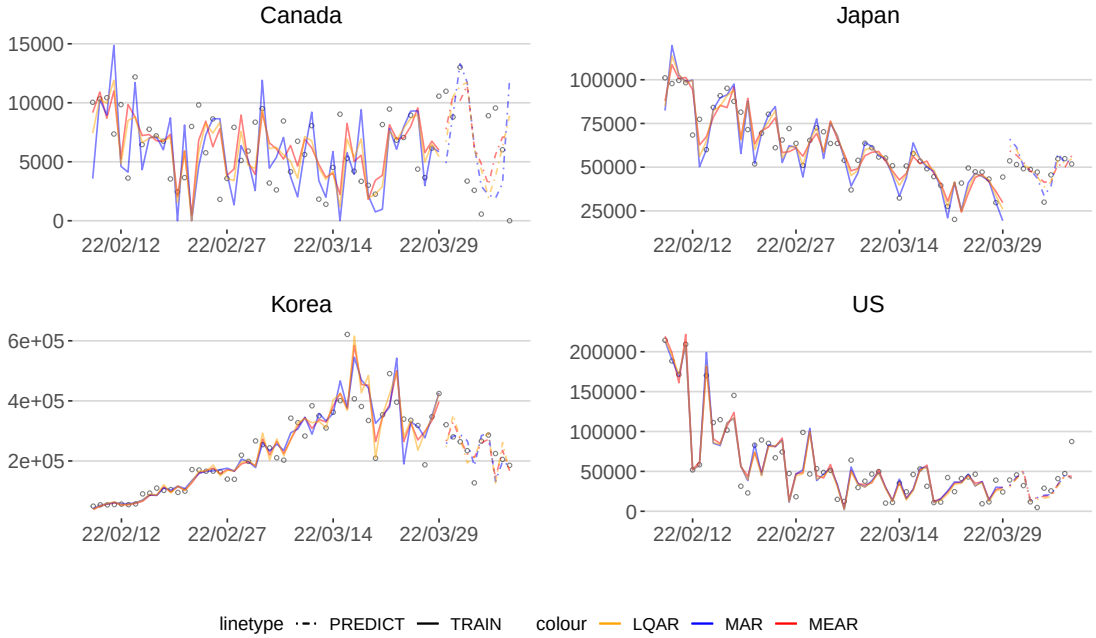

Figure 9: THE QUALITATIVE FORECASTING RESULTS OF THE THE MEAR, LQAR AND MAR METHODS ON THE DAILY CONFIRMED CASES. The red, orange, and blue line represent the forecasting made by the MEAR, LQAR, and MAR methods, respectively using the teacher-forcing method and Silverman's bandwidth.